NAVAL POSTGRADUATE SCHOOL
Monterey, California

THESIS

SPECTRUM ANALYSIS OF INERTIAL AND SUBINERTIAL MOTIONS
BASED ON ANALYZED WINDS AND WIND-DRIVEN CURRENTS
FROM A
PRIMITIVE EQUATION GENERAL OCEAN CIRCULATION MODEL

by

Nicholas D. Gural

December 1982

Thesis Advisor: R. L. Haney

SECURITY CLASSIFICATION OF THIS PAGE (When Data Entered)

REPORT DOCUMENTATION PAGE

READ INSTRUCTIONS BEFORE COMPLETING FORM

1. REPORT NUMBER	2. GOVT ACCESSION NO. / 3. RECIPIENT'S CATALOG NUMBER
4. TITLE (and Subtitle): Spectrum Analysis of Inertial and Subinertial Motions Based on Analyzed Winds and Wind-driven Currents from a Primitive Equation General Ocean Circulation Model	5. TYPE OF REPORT & PERIOD COVERED: Master's Thesis, December 1982 / 6. PERFORMING ORG. REPORT NUMBER
7. AUTHOR(s): Nicholas D. Gural	8. CONTRACT OR GRANT NUMBER(s)
9. PERFORMING ORGANIZATION NAME AND ADDRESS: Naval Postgraduate School, Monterey, California 93940	10. PROGRAM ELEMENT, PROJECT, TASK AREA & WORK UNIT NUMBERS
11. CONTROLLING OFFICE NAME AND ADDRESS: Naval Postgraduate School, Monterey, California 93940	12. REPORT DATE: December 1982 / 13. NUMBER OF PAGES: 73
14. MONITORING AGENCY NAME & ADDRESS(if different from Controlling Office)	15. SECURITY CLASS. (of this report) / 15a. DECLASSIFICATION/DOWNGRADING SCHEDULE

16. DISTRIBUTION STATEMENT (of this Report)

Approved for public release; distribution unlimited.

17. DISTRIBUTION STATEMENT (of the abstract entered in Block 20, if different from Report)

18. SUPPLEMENTARY NOTES

19. KEY WORDS (Continue on reverse side if necessary and identify by block number)

Fourier and Rotary Spectrum Analysis
Modeled Inertial and Subinertial Motion
Primitive Equation General Ocean Circulation Model

20. ABSTRACT (Continue on reverse side if necessary and identify by block number)

The relationship between the applied wind stress and currents predicted by a primitive equation ocean circulation model was analyzed and compared to theory and observations. Three one-year data sets were examined using Fourier and rotary spectrum analysis techniques. The Fourier analysis revealed three spectral peaks in the predicted currents with none in the wind stress. These peaks correspond to synoptic variability at low frequency, the inertial response at an intermediate frequency and a nonphysical response at high frequency, due to the finite time differencing

DD FORM 1 JAN 73 1473 EDITION OF 1 NOV 65 IS OBSOLETE
S/N 0102-014-6601

SECURITY CLASSIFICATION OF THIS PAGE (When Data Entered)

procedure employed. This response at high frequency was two orders of magnitude smaller than the peaks at the synoptic and inertial periods. The inertial motion was the same order of magnitude as the synoptic motion near the surface, but much weaker below. It was identified by the rotary spectrum, and it was slightly shifted toward lower frequencies in direct proportion to the time step used by the model. The Ekman motion appeared to be restricted to the baroclinic response above 70 m. The time-varying "geostrophic" flow below 70 m was essentially barotropic.

Approved for public release; distribution unlimited

Spectrum Analysis of Inertial and Subinertial Motions Based on Analyzed Winds and Wind-Driven Currents from a Primitive Equation General Ocean Circualtion Model

by

Nicholas D. Gural
Lieutenant, United States Navy
B.S., Florida Institute of Technology, 1975

Submitted in partial fulfillment of the
requirements for the degree of

MASTER OF SCIENCE IN METEOROLOGY AND OCEANOGRAPHY

from the

NAVAL POSTGRADUATE SCHOOL
December 1982

ABSTRACT

The relationship between the applied wind stress and currents predicted by a primitive equation ocean circulation model was analyzed and compared to theory and observations. Three one-year data sets were examined using Fourier and rotary spectrum analysis techniques. The Fourier analysis revealed three spectral peaks in the predicted currents with none in the wind stress. These peaks correspond to synoptic variability at low frequency, the inertial response at an intermediate frequency and a nonphysical response at high frequency, due to the finite time differencing procedure employed. This response at high frequency was two orders of magnitude smaller than the peaks at the synoptic and inertial periods. The inertial motion was the same order of magnitude as the synoptic motion near the surface, but much weaker below. It was identified by the rotary spectrum, and it was slightly shifted toward lower frequencies in direct proportion to the time step used by the model. The Ekman motion appeared to be restricted to the baroclinic response above 70 m. The time-varying "geostrophic" flow below 70 m was essentially barotropic.

TABLE OF CONTENTS

LIST OF FIGURES

LIST OF TABLES

ACKNOWLEDGEMENT

I would like to thank Mr. Dennis Mar at the W. R. Church Computer Center, Naval Postgraduate School, Monterey, Ca. for his assistance and guidance in installing the updated version of the BMDP, P-series library, for creating a special procedural file to allow access to the spectrum analysis procedure I needed and also for helping me understand its use. I would further like to express my appreciation and thanks to Dr. C. N. K. Mooers for his guidance and constructive suggestions during the course of my research. His input was quite beneficial in selecting and utilizing the analysis techniques used to study the model features in question.

Finally, I would like to extend my sincere graditude and appreciation to Dr. R. L. Haney for his assistance and support when I was forced to change my research topic in midstream. His patience, guidance and criticism were invaluable during this analysis effort. They were the key to completing this project during the allotted time.

I. INTRODUCTION

Traditionally, general ocean circulation models have been verified against the temperature or density structure of the ocean. This approach was mainly established because of the availability of ocean measurements. Temperature and density, through salinity values, are the ocean variables recorded over the largest area of the world's oceans today. As the number of bathythermograph recordings and ocean stations increased, a pool of temperature and salinity measurements became available, forming a general oceanic climatology which could be used to gauge an ocean circulation model's performance. Once reasonable confidence was established in the model's capability to reproduce known ocean thermal and/or density characteristics, sensitivity experiments could be conducted to test the effects of certain changes in various model parameters on different modeled features.

Since the ocean is a vast sensible heat source or sink for the atmosphere, ocean circulation modeling is not a field unto itself, but it is also tied to improve atmospheric modeling. This is a two way link because both fluids can be modeled by the same general set of physical equations

and, depending on the time scale examined, each forces the other in their overall joint circulation. As a result, a better understanding of the ocean's thermal structure, especially its upper profile and effects which modify it, could lead to improvements in an oceanically coupled atmospheric circulation model over the relatively data sparse areas of the world's oceans.

The objective of this thesis is to analyze the currents predicted by an ocean circulation model as part of a general model verification program. This analysis is expected to improve the ability to model and predict changes in the ocean's motion, thermal fields and its response to atmospheric forcing on a weekly to seasonal time frame. Besides their own intrinsic importance, currents play an important roll in influencing the thermal structure in the ocean. In this respect, their contribution may be twofold: turbulent mixing and large-scale advection. Strong shear currents are responsible for turbulent mixing through convection, while the large-scale Ekman/geostrophic flow contributes to advection. Besides improving its thermal profile, an ocean circulation model which correctly depicts mass transport would have a greater overall applicability than one which is just

concerned with displaying the thermal structure of a water column.

One of the reasons currents have not been examined in verification studies earlier was the lack of available open ocean current data. But as part of NORPAX (North Pacific Experiment), a data base of open ocean long-term currents is now becoming available, McNally (1981). As part of this ongoing experiment, Gerald J McNally of Scripps Institute of Oceanography, La Jolla, California placed a number of drifters, both drouged at various depths and undrouged, in the North Pacific Drift Current. Each buoy was equipped with a transmitter and was tracked for as long as six months by RAMS (Random Access Measurement System) onboard NIMBUS 6. Several results of this ongoing investigation are now available. One, the apparent lack of difference between current observations at the surface and at 30 m, will serve as a good test for examining the current profile produced by an ocean circulation model. The observed statistical relationship between winds and currents also needs to be investigated from a theoretical or modeling point of view.

II. MODEL DESCRIPTION

The model evaluated was developed by Robert L Haney, Naval Postgraduate School, Monterey, California (Haney et al, 1978). It is a primitive equation model applied to a baroclinic ocean in a rectangular basin. It contains 20 levels in the vertical with 8 in the upper 200 m. The model is based on the hydrostatic and Boussinesq approximations. A rigid-lid approximation is made at the surface and salinity is neglected. The effects of subgrid or mesoscale motion are parameterized by vertical and nonlinear horizontal eddy viscosities and conductivities.

The model is driven by heating and stresses applied at the surface. The downward flux of heat and momentum is determined by the following time-dependent variables: the predicted ocean surface temperature, the prescribed values of 6-hourly surface winds and monthly mean: air temperature, specific humidity, fractional cloud cover and incoming shortwave radiation. These quantities are used to calculate the shortwave and longwave radiation, sensible and latent heat and surface wind stress. The bulk aerodynamic

equations for determining wind stress from marine winds along with the primitive equations of motion, the continuity equation, the first law of thermodymanics and the equation of state can be found in Haney, et al (1978). The governing solar radiation equations can also be found in this reference with one exception. A new approach as outlined in Haney (1980) allows some of the solar radiation to penetrate to depths greater than 20 m rather than being totally absorbed in this layer as was the case with the old radiation equation.

To handle the transport of heat and momentum which occurs on scales too small to be resolved by the grid spacing employed, parameterizations of these motions are made on scales which are discernible by the model. Since eddy flow is important, especially in western boundary currents and their extensions, this motion must not be neglected in an ocean circulation model. Until model grids are reduced to a size sufficiently small to allow eddy representation, various theories must be applied to approximate eddy motion. The Haney model uses the mixing length and momentum hypothesis of classical turbulence theory. This approach introduces coefficients of horizontal eddy viscosity and

conductivity. Vertical diffusion is approximated through small coefficients of vertical eddy viscosity and conductivity, see Haney, et al (1978).

Active turbulent vertical mixing of heat and momentum in the model is based on a parameterized "dymanic adjustment". The key to the adjustment is the local gradient Richardson number. This number is a non-dimensional measure of stability as it relates the local hydrostatic stability or density stratification to the square of the local shear. When the water column is neutral, the local Richardson number takes on its critical value of 0.25. This value was theoretically established and is justified through observations presented in Thompson (1980). The adjustment consists of checking the water column at all levels below the surface for dynamic instability. This condition exists if the local gradient Richardson number computed between two adjacent model levels falls below its critical value. In this case, a vertical mixing of both temperature and velocity components between the adjacent levels transpires in such a way that: (a) heat and momentum are conserved, (b) the mixing ratios for heat and momentum are set equal and (c) the adjusted gradient Richardson number is set equal to its critical value. The

specifics of this adjustment procedure can be found in Adamec, et al (1981). It is through this parameterized mixing mechanism that the model predicted currents affect the vertical turbulent mixing of both heat and momentum. This is because the gradient Richardson number depends on the square of the shear of the model predicted currents.

Baroclinic (or shear) currents are handled through direct calculations from the horizontal equations of motion. The vertically averaged currents are defined by a streamfunction derived by a vertical average of the horizontal equations of motion and governed by the vorticity equation. These average currents are then added to the results of the primitive equations to yield the total currents. The model runs on a staggered grid with the temperature and streamfunction gridpoints established at the model indices and momentum gridpoints offset by half a grid length. Time differencing is accomplished by using the leap-frog scheme with a Euler-backward scheme inserted every 8 timesteps to reduce "time-splitting".

The rectangular domain covered in the model is in the North Pacific. It is 90° of longitude in width, running from 145° E to 125° W and is 65° of latitude in length,

running from the equator to 65° N. This domain allows the model to simulate the circulation pattern of the interior North Pacific Ocean. The general surface flow includes the equatorial flow pattern, the North Pacific gyre and the Subpolar gyre systems. The complex flow around the Japanese and Aleutian Islands are not revealed because these intruding land masses are not included in the boundary conditions. The bottom is flat at a uniform depth of 4 km. At the lateral boundaries, there is perfect insulation of both heat and momentum with zero velocity except at the equator where a free slip condition is imposed. The bottom is also thermally insulated but a small stress is imposed through a simple quadratic drag law, see Weatherly (1972).

III. MODEL OUTPUT

A. MODEL INITIALIZATION AND SIMULATION

The model simulation was primarily driven by 10 years (from 01 Jan 1969 through 31 Dec 1978) of 6-hourly marine wind analyses performed by FNOC (Fleet Numerical Oceanography Center, Monterey, California). These winds are the variable input to the bulk formula used to calculate the surface wind stress and the latent and sensible heat fluxes in the model. The other atmospheric forcing variables: solar radiation, cloud cover, air temperature and vapor pressure; are all prescribed by monthly climatological values. The sources of these values are given in Haney, et al (1978).

The model started from an initial state with zero currents and a temperature structure which decreased linearly with depth ranging from a value equal to the local air temperature at the surface to 2° C at the bottom. It then ran for 3.5 years from 01 Jan 1974 through 30 Jun 1977 with the forcing being supplied by the FNOC wind analyses and the monthly atmospheric climatologies. During this initial

phase, the model used 25 fixed levels in the vertical (12 in the upper 200 m) running on a coarse grid with a spacing of approximately 6° of longitude and 4° of latitude.

After this initial "spin up" was complete, the model was run to simulate three decades of ocean circulation using the 10 years of wind data available. The first 10 years of simulation was run on a coarse grid (6°x4°) and the succeeding 20 years were run on a fine grid (3°x2°). Each time a new decade of simulation was started, a smoothing was applied to the model variables (currents and temperatures) in order to reduce "model shock" when the wind forcing was shifted back to 01 Jan 1969. This smoothing consisted of averaging the simulated variables over the last 2 weeks of that particular decade and using these average values when the model was reinitialized to Jan 1969 to start the next decade of simulation. When the model was switched to the fine mesh grid, the grid size was cut in half and values were linearly interpolated to the new gridpoints.

B. COARSE GRID OUTPUT

The coarse grid used for the initial decade of ocean simulation consisted of 17 points in both the longitudinal and latitudinal direction. As a result, the grid spacing

was approximately 6° of longitude and 4° of latitude. The model was run with 20 levels in the vertical vice the 25 levels used in the initialization phase. The levels used in this simulation (for both the coarse and fine grid) were as follows: 5, 16.5, 31, 49, 71.5, 100, 136.5, 182.5, 240, 313, 405.5, 522, 669, 855, 1090, 1385, 1760, 2235, 2830 and 3580 m below the undisturbed surface.

The variable coefficents of horizontal eddy viscosity and conductivity as displayed in Haney, et al (1978) come from the following equation -

$$A = A_o \left[1 + \gamma |\nabla \zeta| (\Delta s)^3 \right] \qquad (1)$$

where ζ is the relative vorticity of the vertically averaged current and ΔS represents a constant which is a measure of the grid size. In the present model $\gamma = 4 \times 10^{-8}$ sec/cm^2. For the coarse grid, the background value for momentum is $A_o = 5 \times 10^8$ cm^2/sec and for heat is 1×10^8 cm^2 /sec. The vertical eddy viscosity is $K_M = 5$ cm^2 /sec and conductivity is $K_H = 0.5$ cm^2/sec . The coarse grid is run using a 6 hour time step.

During this first decade, one sample of model output for all levels in the vertical at a single gridpoint was extracted for analysis. The gridpoint choosen was located

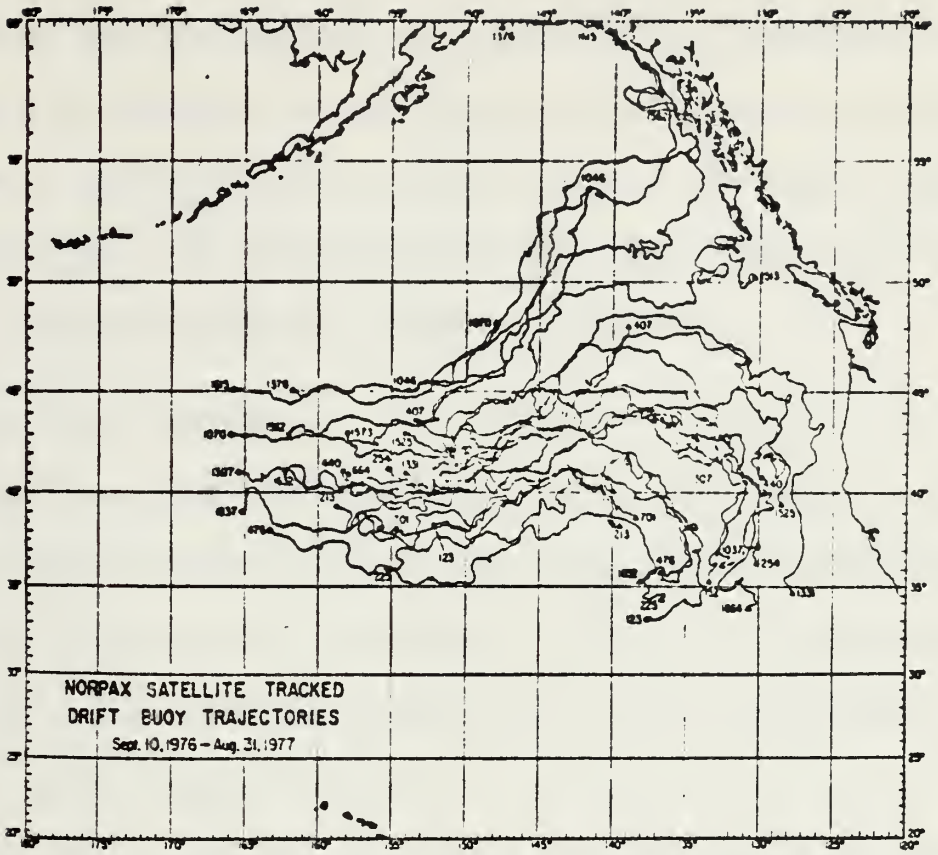

Figure 1. Gridpoint Position Relative to NORPAX Drifter Data.

at 42.66° N and 150.31° W. See Fig. 1. The analysis period went from 01 Jul 1976 00Z through 30 Jun 1977 18Z. This time frame and location was choosen for a preliminary analysis of the model's reponse because it corresponds to the space and time domain of the drifter data collected by G. J. McNally for NORPAX and is in the major strom track across the North Pacific. It is possible that the initialization of the model and the transition to the first decade affected

the quality of the output used in the analysis. But since the model had run through 8.5 years of continuous simulation before the output was extracted, and because the analysis was only conducted down to 313 m, it was felt that any influence of the initial conditions would have long since been dispersed from the current structure.

C. FINE GRID OUTPUT

The fine grid representation was established to improve the horizontal resolution of the predicted variables and the inertial response in the model. This was accomplished by reducing both the grid spacing and the time step used in the finite differencing scheme.

The fine mesh version uses 33 gridpoints in both the longitudinal and latitudinal directions. This reduces the grid spacing to approximately 3° of longitude and 2° of latitude or twice the resolution of the coarse grid. Once again, a staggered grid is used with the temperature values determined at the model indices and the momentum values offset by half a grid length. The time step used in integration was also halved to 3 hours to maintain linear computational stability.

The only other change is in the magnitude of the horizontal eddy viscosity and conductivity coefficients. These constants are reduced by a power of ten to a value of $A_o = 5 \times 10^7$ cm^2/sec for viscosity and 1×10^7 cm^2/sec for conductivity. The governing equation may be found in the previous section covering the coarse grid.

All the other model parameters and criteria are the same as the coarse grid version. The same 20 levels are used for vertical resolution. The relatively small coefficients of eddy viscosity and conductivity in the vertical have also been left unaltered.

The fine mesh simulation of ocean circulation consisted of two decades of model execution. After the two week average from the end of December 1978 was applied to the coarse grid at the conclusion of the first decade modeled, the grid length was converted to the fine mesh length. A linear interpolation of the averaged u and v currents and temperatures was performed to assign values to the newly created intervening gridpoints. The second decade of current simulation was then conducted reusing the 10 years of marine wind analyses supplied by FNOC. To use a 3-hour time step in the fine mesh run, a linear interpolation of the 6-hourly

synoptic winds was performed. The other atmospheric forcing parameters still came from the same monthly climatology as used in the coarse grid run.

When the second decade (first with the finer resolution) was completed, a third decade was run. Once again, the two week average smoothing procedure was employed on the ocean variables between decades before the winds were reinitialized to 01 Jan 1969. It was from this third decade of simulation that the two fine mesh samples of model output for data analysis.

The first fine grid data set ran from 01 Jul 1969 03Z through 01 Jul 1970 00Z. It consisted of a single gridpoint with all the values in the vertical being extracted as in the coarse grid case. The gridpoint extracted in this case was located at 43.67° N and 148.91° W. See Fig. 1. The analysis of this data allowed an interannual comparison in studying the model's fine mesh performance.

The final data set matched the timeframe and general location of the coarse grid set. It was located at 41.64° N and 151.72° W. See Fig. 1. This set was studied in the greatest detail in an attempt to understand the model's response and compare it to some of the preliminary results available from the NORPAX drifter data.

IV. RESULTS

A. ANALYSIS PROCEDURES

Each model data set extracted from the simulation was analyzed using a new Biomedical Computer Program, P-series subroutine, BDMP1T - Univariate and Bivariate Spectral Analysis. This program package became available in the beginning of 1982. It uses cosine transforms in a fourier analysis approach to reduce input data into its spectral components at all the analyzable frequencies, from 0.0 to 0.5 (the Nyquist frequency). The subroutine's output frequencies are dimensioned per unit data time step and as a result must be converted to be meaningful to the particular data set analyzed. The spectral package runs its analysis using three different bandwidths: narrow, medium and wide. These bandwidths may either be individually specified or assigned by the program if left to the default mode. In the default mode, the bandwidth size is dependent on the number of values in the input data set. Since this study was only concerned with the large-scale trends displayed by the Haney general circulation model, only the widest bandwidth results

were utilized. These results were also the smoothest curves produced by the subroutine and are statistically the most stable. For a complete description of this program package, refer to Engelman, et al (1981). This spectral option was chosen over the other program libraries available at the Naval Postgraduate School because of the ease in interpreting its output, variety of analysis options available, detailed description in the user's manual and clarity in diagnostic messages produced.

A detailed analysis of the fine mesh 1976-77 data set was performed. It involved a description of the temperature and stability profile of the simulated upper ocean over the annual cycle, a spectrum analysis of the predicted currents, a lowpass spectral analysis to examine the model's wind/current relation and a rotary spectrum analysis to examine its inertial response. The lowpass analysis was a two step process. First, the model current data was run through an eleven-point lowpass filter to remove the energy above the inertial frequency as determined by the original spectrum analysis. The weights used by this lowpass filter were: 0.0166, 0.0402, 0.0799, 0.1231, 0.1561, 0.1684, 0.1561, 0.1231, 0.0799, 0.0402, 0.0166. After lowpass filtering,

the 3-hourly data was resampled twice a day and spectrally analyzed once again. This procedure resulted in increasing the discernible analysis range produced by the Biomed spectrum analysis package. With a sampling interval of 12 hours, the analysis period was increased to 1 to 20 days as compared to the 6 to 120 hour range depicted by the 3-hour time step data of the general study. The relationship between the input wind stress and near surface currents was then examined at this extended frequency range.

The rotary spectrum analysis produced a decomposition of the model spectral currents into their cyclonic and anticyclonic components. This procedure utilized the autospectrum of the u and v current components and their quadrature spectrum at each of the model levels studied. The result of this analysis is a ratio of the cyclonic to anticyclonic circulation which can then be compared to the theoretical ratio using the analyzed frequencies and the inertial frequency. According to theory (Mooers, 1973), the value of this ratio approaches one at the very highest and lowest frequencies (compared to the inertial frequency) and is zero at the inertial frequency. Because of this, the model's inertial frequency will be indicated by a minimum in the ratio. The equation used is -

$$R(s) = \frac{S(s)}{S(-s)} \qquad (2)$$

$$= \frac{(s-f)^2}{(s+f)^2} \qquad (3)$$

the cyclonic spectrum: $S(s) = 0.5\,(Guu(s)+Gvv(s)+2Quv(s))$

anticyclonic spectrum: $S(-s) = 0.5\,(Guu(s)+Gvv(s)-2Quv(s))$

where $s \geq 0$ is a given frequency, f is the inertial frequency, Guu(s) and Gvv(s) are the autospectra of u and v respectively and Quv(s) is the imaginary part (quadrature spectrum) of the cross spectrum between u and v.

The results of these analysis procedures will be described and interpreted in the following sections. The first data set treated is the fine mesh 1976-77 data. A general description of the relevant model characteristics will be presented, followed by the spectrum analysis results. The model's inertial frequency will then be discussed, followed by supporting results from the rotary spectrum. Then the wind/current relation will be presented using the lowpass filtered analysis.

Once the analysis of the 1976-77 fine mesh data is presented, a comparison will be made with the 1969-70 fine mesh data. After this comparison, the 1976-77 data set will be

compared to its coarse grid counterpart. The results suggest there is little difference between the two different years of fine mesh data but some important differences between the coarse and fine grid data sets exist.

B. FINE MESH RESULTS

1. General Description of Some Output Parameters

Each of the data sets was analyzed at four model levels: level 1 (5 m, called the surface level in the resluts), level 3 (31 m), level 5 (71.5 m) and level 10 (313 m). These particular levels were chosen to discern the model's characteristics through its approximate mixed layer representation, in the transition zone or thermocline below the surface mixed layer and in the interior of the model. This decomposition of the water column at the gridpoint selected is supported by the temperature, stability and current structure produced by the model.

The temperature structure during 1976-77 is displayed in Fig. 2. It shows a typical mixed layer structure going from a very warm, shallow (approximately 10 m) mixed layer in the summer months of June, July and August to a deep isothermal layer in the winter and early spring, approximately February through April. The mixed layer

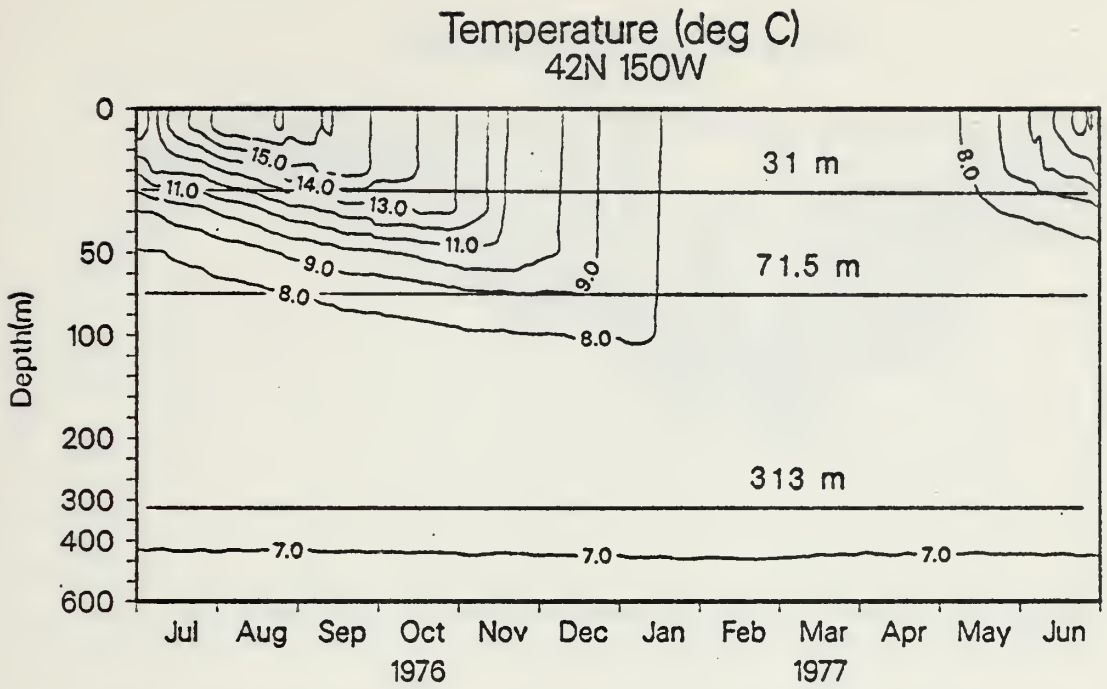

Figure 2. Fine Mesh Temperature Structure (JUL 76 - JUN 77).

extends to at least 30 m from October through May supporting the selection of 30 m as a good depth for approximating the central part of the mixed layer. The selection of depth 71.5 m as the mean transition zone is supported by the location of seasonal thermocline, which is below 71.5 m from August through January. The seasonal thermocline does not reach that depth in the summer and vanishes in the winter, as expected. At 313 m, the temperature is relatively constant throughout the year, placing it below the surface thermal effects and indicating that it represents the common water in the interior of the model ocean.

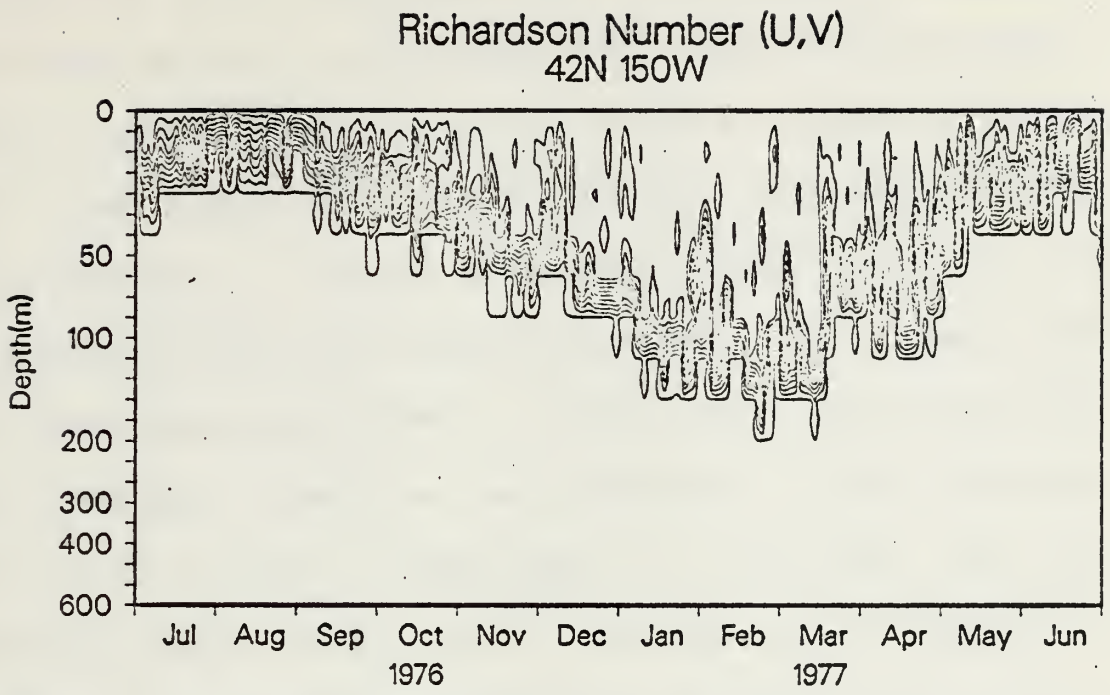

Figure 3. Richardson Number based on Total Currents for Fine Mesh Model (JUL 76 - JUN 77).

The dymanic stability of the water column, as represented by the Richardson number, also supports the thermal structure breakdown criterion selected. Fig. 3 shows the gradient Richardson number (Ri) in increments of 0.5 based on the total current, where -

$$R_i = \alpha g \frac{\partial T}{\partial z} \Big/ \left[\left(\frac{\partial u}{\partial z} \right)^2 + \left(\frac{\partial v}{\partial z} \right)^2 \right] \qquad (4)$$

and α is the thermal expansion coefficient, g is the gravitational acceleration and T is the temperature. The contour intervals plotted represent Ri=0.5. The smallest value

contour of Ri=0.5 indicates that the turbulent portion of the water column is above this line. The critical value of Ri=0.25 (where the water column becomes neutral) lies in this upper region and marks the base of this surface turbulent structure. As the Richardson number increases, the stability of the water column increases. The largest value contoured represents Ri=5.0. Using the depth of the critical Richardson number as an indication of the transition zone below the well mixed layer, it is noted that this level is deeper than 71.5 m in the winter and shallower in summer. This shows the selection of 71.5 m as an average for the transition zone was reasonable. The importance of the shear of the inertial motion in determining the stability can be displayed using a plot (Fig. 4) of the gradient Richardson number calculated from averaged currents with the interial frequency removed. As can be seen, the unstable zone does not penetrate as deeply as it does in Fig. 3. The depth of turbulent mixing that would exist in the absence of inertial motion is somewhat less according to this comparison. Thus, these motions make an important, though perhaps not crucial, contribution to the turbulent mixing in this model.

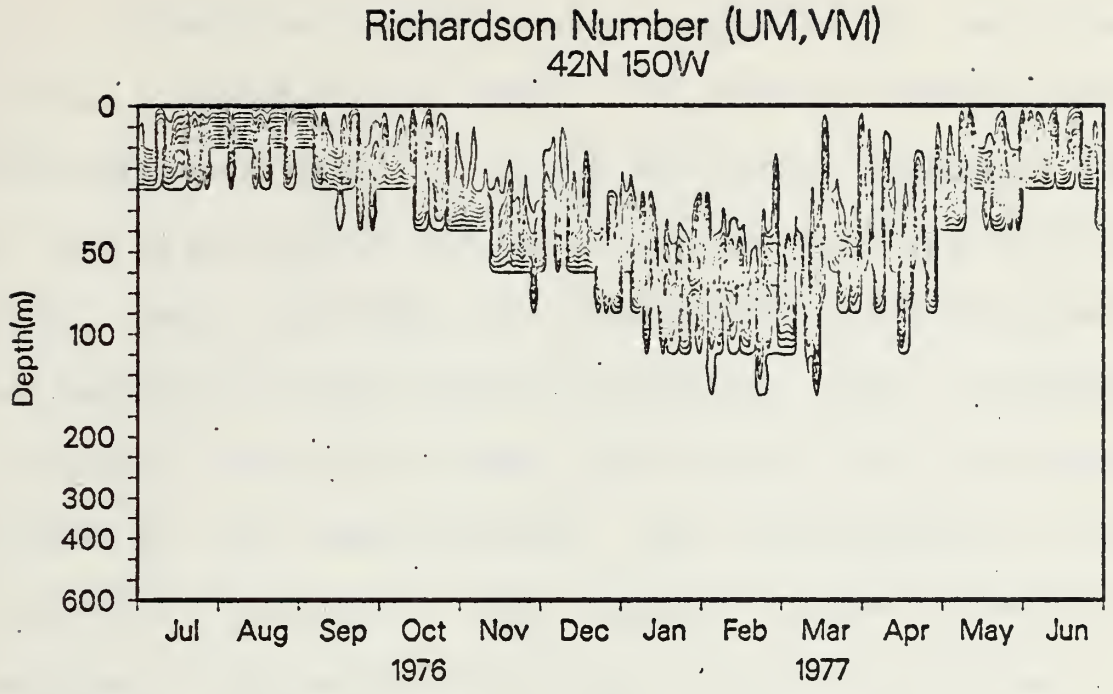

Figure 4. Richardson Number based on Mean Currents with Inertial Components Removed for Fine Mesh Model (JUL 76 - JUN 77).

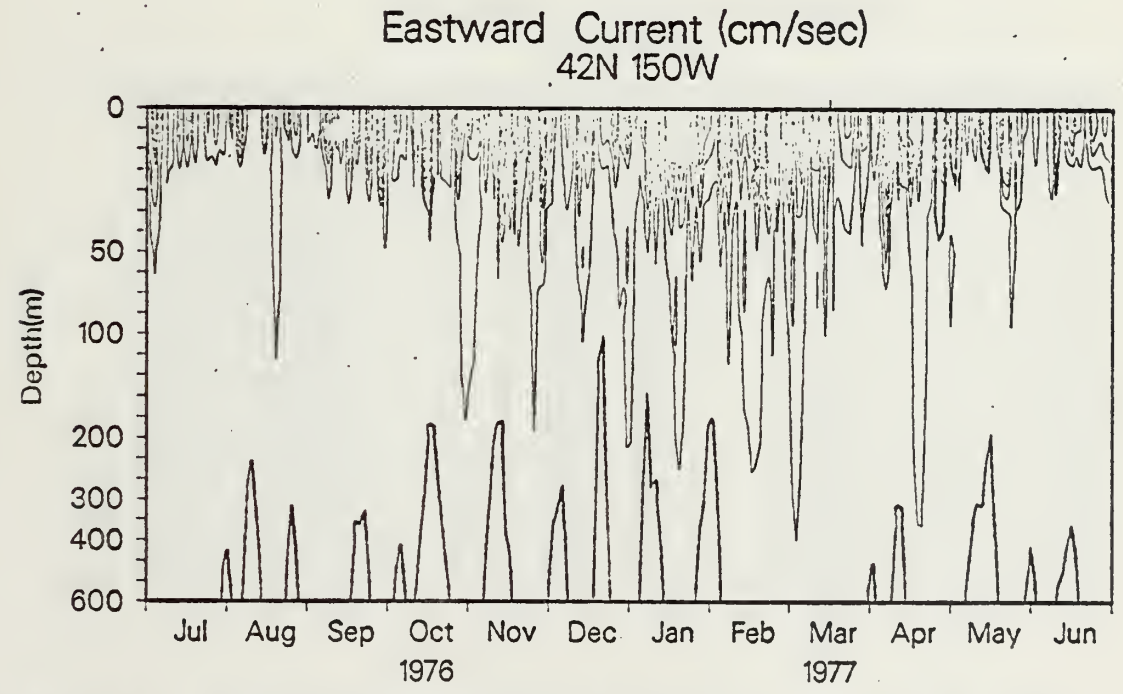

Figure 5. East-West Current Component from Fine Mesh Model (JUL 76 - JUN 77).

The above result is also supported by the current profile produced by the model. As seen in both the east-west component, Fig. 5, and the north-south component, Fig. 6, the major current fluctuations occur above approximately 30 m. Below this depth, the currents show little change in the vertical and are reduced in magnitude. Fig. 6 displays a periodic direction reversal below about 70 m, as demonstrated by the heavy vertical line representing a zero north-south velocity. This pattern depicts a basically barotropic response below the mixed layer which is also seen in the spectrum analysis presented in the next section.

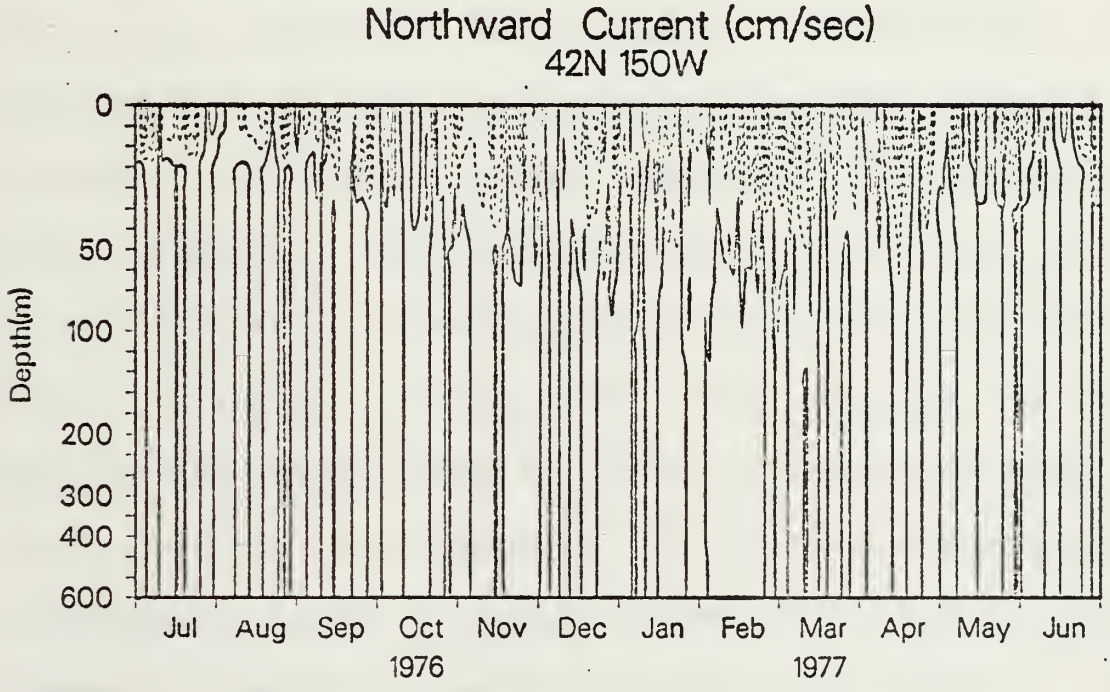

Figure 6. North-South Current Component from Fine Mesh Model (JUL 76 - JUN 77).

2. Spectrum Analysis

A spectral analysis of both the input wind stress and the currents produced by the model was made. The bandwidth used was 0.2816 cycles/day (cpd). The wind stress as seen in Fig. 7 was analyzed to determine if a spectral peak was present which could be transmitted to the ocean and show up in the current simulation. With no peak found, it can be safely assumed that any spectral peak in the currents is not a direct result of the wind stress forcing and must be due to some oceanic "natural selection" process. Figs. 8 and 9 display the power spectrum of the u and v current components, respectively. Three spectral peaks can be seen. The first is at relatively low frequency and represents the transient flow produced by atmospheric synoptic forcing in the model. This peak will be examined in the wind/current relation section. The barotropic motion in the interior of the modeled water column displayed in Fig. 6 is represented by this portion of the spectrum. At frequencies less than 0.30 cpd, the energy levels at level 5 (71.5 m) and level 10 (313 m) are the same indicating that most of the energy in this frequency range is confined above 71.5 m and the model response is basically barotropic below this depth. The

upper portion of the ocean displays baroclinic conditions in contrast to this barotropic response in the model interior. At the lowest frequencies (≤0.1cpd), the energy spectra in u and v are of the order of 2.653×10^{3} and 1.761×10^{3} at the surface and 5.679×10^{1} and 3.799×10^{1} cm^2/sec^2 at 71.5 m and below, respectively. This indicates RMS currents at these frequencies of about 27.3 and 22.3 cm/sec at the surface, with 4.0 and 3.3 cm/sec at 71.5 m and below.

The dominant peak in the spectrum is centered in the 0.9576 - 1.0256 cpd range. Its amplitude is of the same order of magnitude as the low frequency peak in the upper three levels analyzed. This peak is also evident at 313 m, but here its amplitude is much smaller than that of the low frequency motion. Since the inertial frequency represents a high energy level in the ocean compared to the frequencies around it, it is concluded that this peak is the model's inertial response. This response is discussed in greater detail in the next section. The last peak visible is very small in amplitude, located at relatively high frequency and appears only in the upper levels studied. This peak is outside the objectives of this study and is only investigated because of the marked effect in the rotary spectrum

associated with it. It appears at a frequency corresponding to a period roughly 2.5 times the model time step. It is felt this high frequency peak is an artifact of the finite difference scheme and not the result of any real physical phenomenon. Because it is at least two orders of magnitude smaller than the other significant features in the model, the overall effect of this peak on the model's performance should be small.

3. Inertial Motion

Using the coriolis parameter calculated from the latitude of the gridpoint as input, the inertial period is 1.3289 cpd. The model's inertial response lies in the 0.9576 - 1.0256 cpd range according to the spectral results and is further refined by the rotary spectrum to 1.0256 cpd. This shift toward lower frequencies appears to be due to the trapezoidal implicit time differencing scheme employed by the model and is directly dependent on the length of the time step used (see comparison with coarse grid model below).

As stated in the previous section, the inertial motion in the ocean will be associated with a dominant spectral peak when the currents are studied over a year. This

Figure 7. Energy Spectrum of Applied Wind Stress in Fine Mesh Model (JUL 76 - JUN 77).

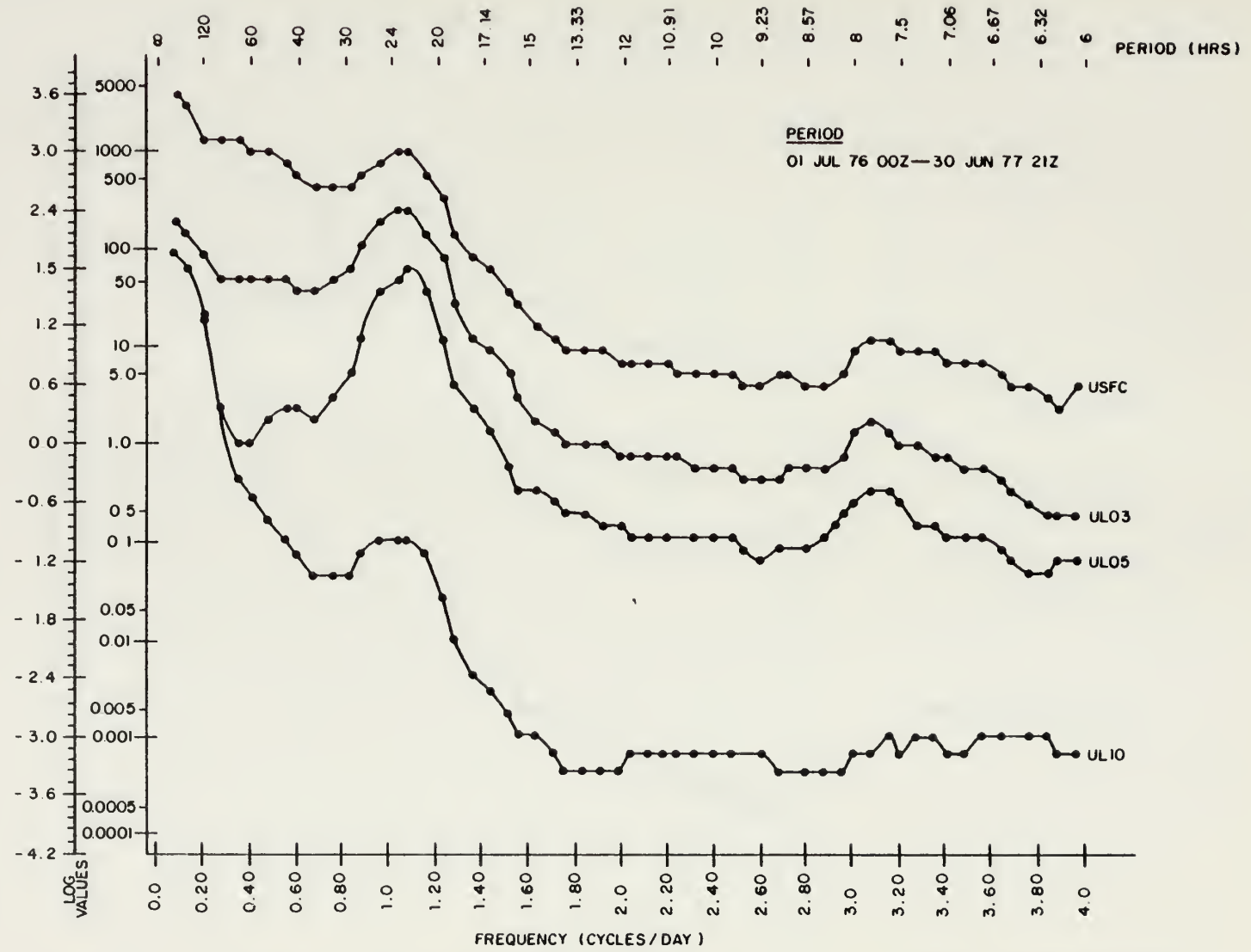

Figure 8. Energy Spectrum of U-Component Current in Fine Mesh Model (JUL 76 - JUN 77).

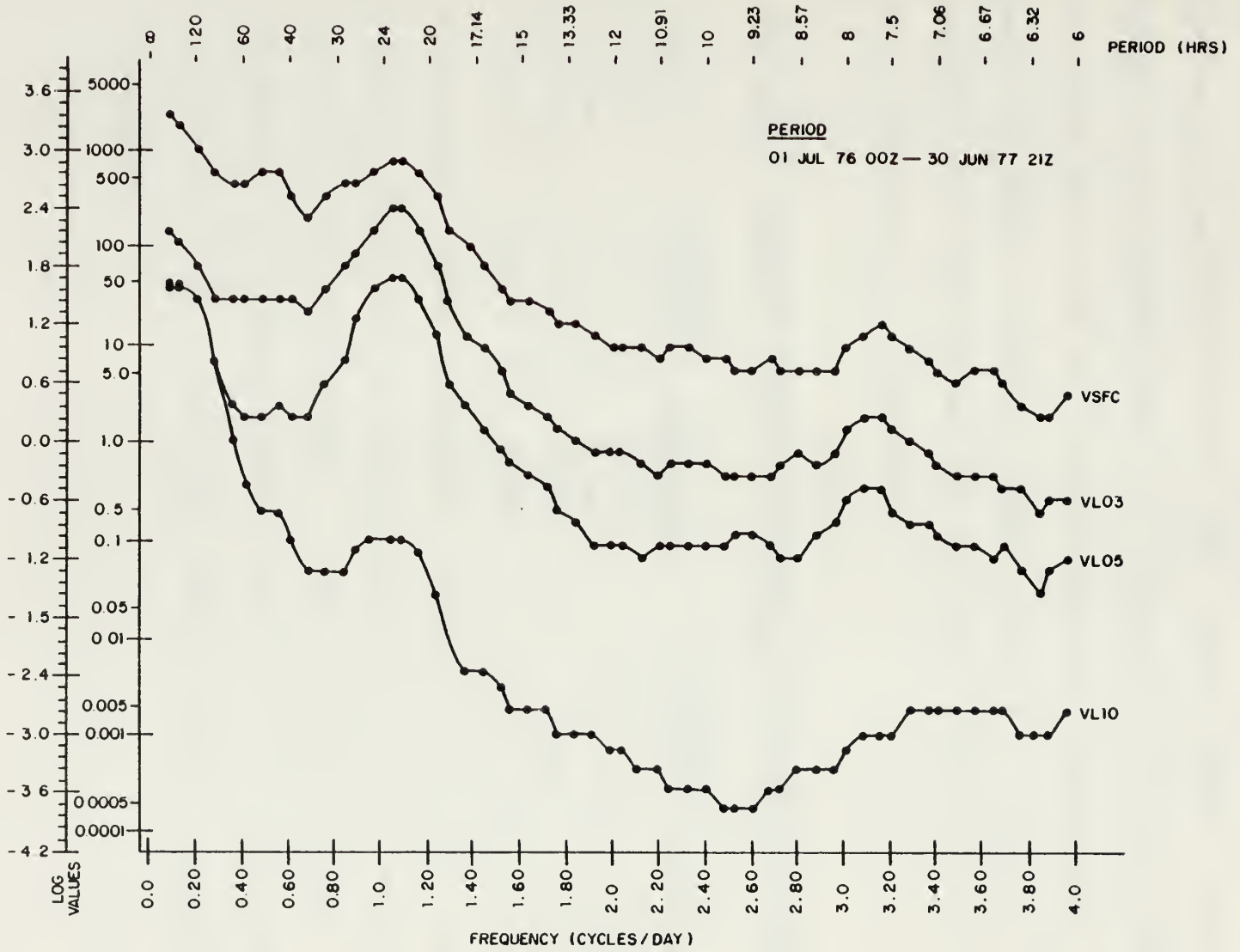

Figure 9. Energy Spectrum of V-Component Current in Fine Mesh Model (JUL 76 - JUN 77).

is due to the tendency for intermittent ocean motion at the inertial frequency. The signature of inertial motion in the model can be seen in the spectrum analysis through 313 m. The energy associated with this motion appears somewhat masked in the surface level, is dominant in the mid levels and falls off at 313 m. The spectral energy associated with half the height of each inertial peak at 1.0256 cpd is listed in the table below along with the frequency band over which this energy is distributed.

TABLE I

Half Power Spectral Energy (cm^2/sec^2) and Bandwidth (cpd) for Model Inertial Motion for Fine Mesh (JUL 76 - JUN 77).

LEVEL	U-COMPONENT ENERGY	BANDWIDTH	V-COMPONENT ENERGY	BANDWIDTH
sfc (5m)	6.918×10^{2}	0.238	3.981×10^{2}	0.446
L03 (31m)	1.047×10^{2}	0.349	7.943×10^{1}	0.365
L05 (71.5m)	1.096×10^{1}	0.360	7.244	0.376
L10 (313m)	7.244×10^{-2}	0.287	6.607×10^{-2}	0.303

The spectral phase information produced when the u and v components were analyzed shows that the inertial motion in the model was anticyclonic. The v-component leads the u-component by approximately 90° (from 89.7° at the surface to 90.6° at 313 m) for all four levels studied, as expected from theory.

The rotary spectrum confirms this spectral peak as the model's inertial response. The theory behind this analysis approach (Mooers, 1973) dictates that the ratio between the cyclonic and anticyclonic flow components in a water column go to zero at the inertial frequency where the motion is purely anticyclonic. The results of the rotary spectrum calculated from equation (2) for each level analyzed are depicted in Figs. 10 - 13 respectively. The theoretical curve calculated from equation (3) using the actual inertial frequency calculated from the gridpoint's coriolis parameter is also plotted for comparison. It can be concluded from these curves that the model's best performance, according to the supporting theory for the rotary spectrum, is in the frequency range of approximately 0.3 - 2.2 cpd. From the tables of analyzed frequencies used to produce these curves, it can be seen that the minimum in the calculated ratio is at 1.0256 cpd which corresponds to the inertial frequency determined from the spectral analysis covered in the previous section. The tables used in the rotary spectrum may be found in Appendix A. Since most of the model's energy at each level is contained at frequencies lower than 2.2 cpd, its response is generally good when

examined by this method which is based on inertial-internal wave theory, $f < \sigma < N$.

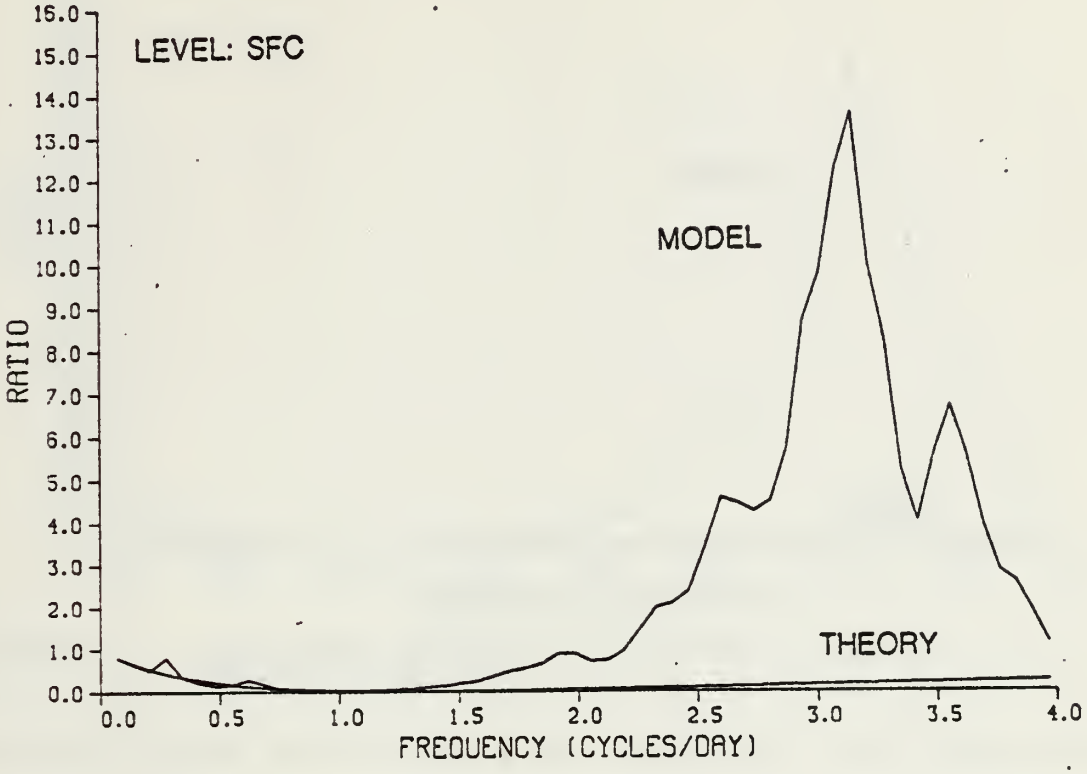

Figure 10. Fine Mesh Rotary Spectrum for Surface (5 m), JUL 76 - JUN 77.

According to the rotary spectrum, the high frequency peak visible in the spectrum analysis (near 3.2 cpd) appears to be associated with strong cyclonic motion at all levels studied. But the RMS velocities at this frequency are: 1.8, 0.7 and 0.3 cm/sec at the surface, 31 m and 71.5 m, respectively. There is no peak evident at 313 m. As alluded to earlier, this motion, having a period near $2\Delta t$, may be the

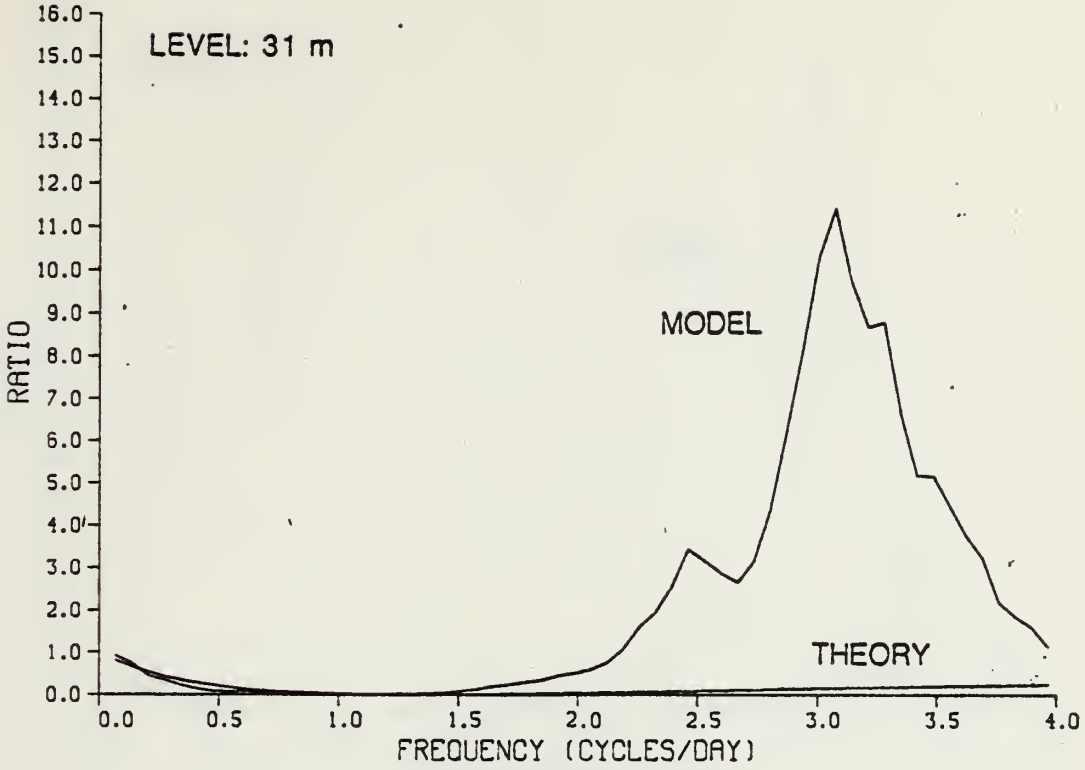

Figure 11. Fine Mesh Rotory Spectrum for Level 03 (31 m), JUL 76 - JUN 77.

result of time splitting in the leapfrog time differencing scheme. The model's performance can be improved if this peak is removed; but because of the very small amount of energy associated with it, its impact on the model's general ocean circulation characteristics should be minimal.

4. Wind/current Relation

The aim of this part of the study is to inspect the model's performance in regards to Ekman theory (wind driven flow to the right of the surface stress in the Northern Hemisphere). Accordingly, the output current structure will

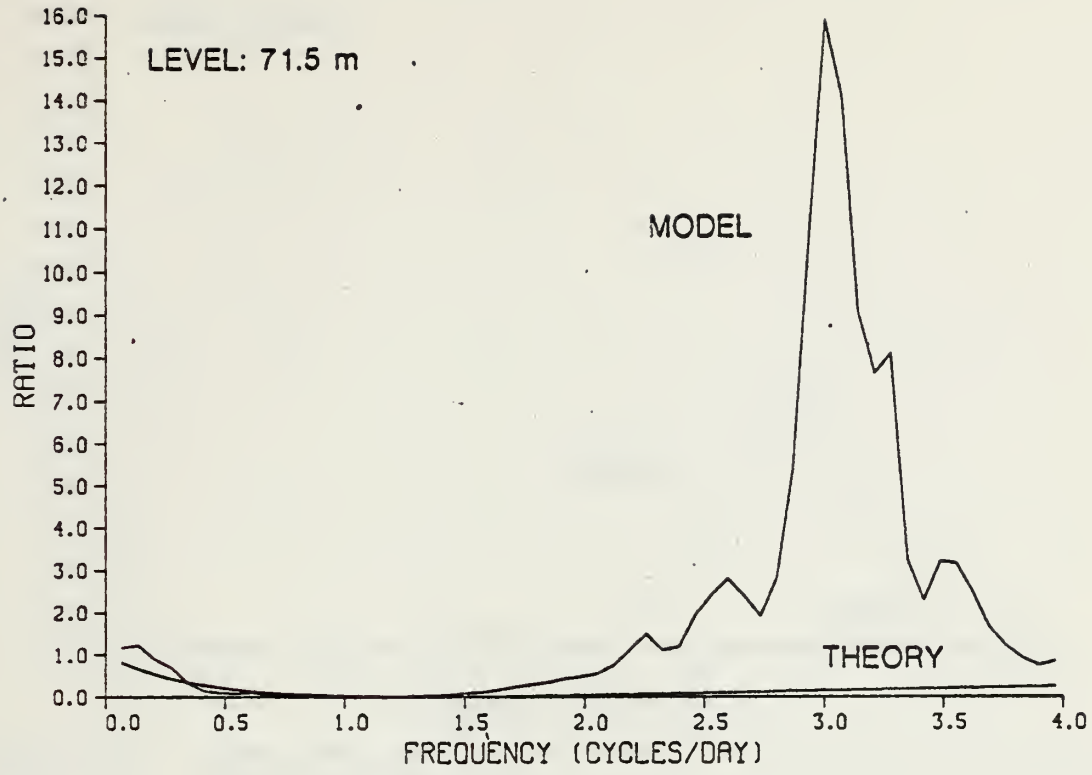

Figure 12. Fine Mesh Rotary Spectrum for Level 05 (71.5 m), JUL 76 - JUN 77.

be examined where there is high coherence between the current and its orthogonal wind stress. The point at which this relation breaks down in going toward high frequencies indicates the limit of steady Ekman response and the transition in governing physics to time dependent Ekman response to the applied wind stress. This transition will be supported by an increase in the coherence with the parallel wind stress. It is also expected that the coherence between the current and its orthogonal wind stress will rapidly decrease with depth below the model's mixed layer, assuming

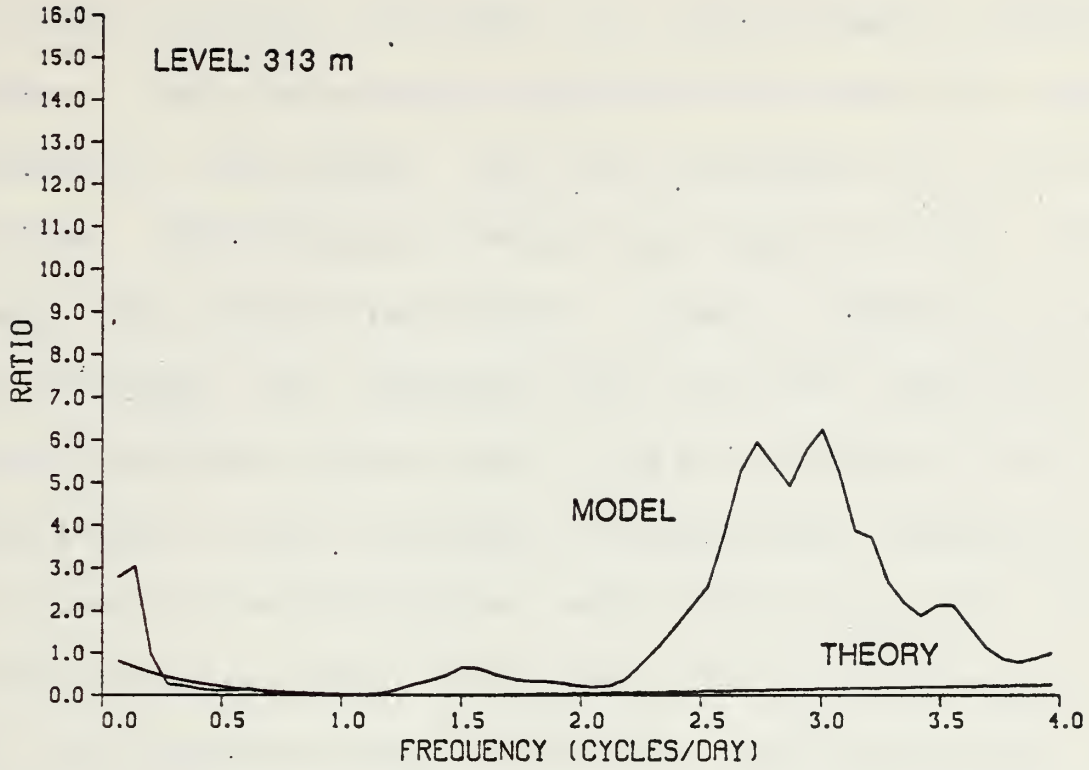

Figure 13. Fine Mesh Rotary Spectrum for Level 10 (313 m), JUL 76 - JUN 77.

this level is a good first order approximation of the Ekman depth. At this depth, the frictional effect of the applied wind stress falls off to 4 percent of its surface value. Below this depth, the geostrophic component of the current should be removed from the flow before an evaluation of any relation between the applied wind stress and currents is made.

The results of the coherence study between the currents at the selected model depths and the applied wind stress using the lowpass filtered data running from 0.05 -

1.0 cpd generally conformed to the hypothesis presented above. The coherence was generally high between the u-component of the current and the y-component of the wind stress. This coherence pattern was mimicked by the v-current and x-wind stress except at lower coherence values. As expected, the coherence falls off with depth with a marked decrease between level 3 (31 m) and level 5 (71.5 m). Recall that level 3 provided a satisfactory indication of the base of the mixed layer when averaged over the entire year of data and level 5 provided a satisfactory indication of the transition zone or seasonal thermocline below the mixed layer. According to the coherence results, it maintains a coherence of less than 0.4 over most of the frequency range examined and therefore appears to be primarily below the Ekman depth in the model. Because of the strong seasonal signal, a spectrum analysis of seasonally stratified data may be beneficial in the future.

The coherence values between the surface u-current and y-wind stress ranged from a high of 0.966 to a low of 0.193. The coherence is over 0.90 in the frequency range from 0.0 - 0.625 cpd and finally drops below 0.80 at 0.87 cpd at level 1 (5 m). After this point, the coherence

continues to fall through the rest of the analyzed frequency range. This overall pattern is reflected in the level 3 (31 m) analysis, only with lower coherence values. The maximum value is reduced to 0.853 with a minimum of 0.090. The values stay above 0.75 from 0.0 - 0.516 cpd and finally drop below 0.65 at 0.90 cpd. This trend completely disappears at level 5 (71.5 m). The coherences are all below 0.375 except at two peaks - one centered at 0.57 cpd, the other at 0.856 cpd. These peaks increase to coherences of 0.650 and 0.575 respectively, and may reflect Ekman pumping/suction. They are also visible at level 10 (313 m). From this analysis, it appears that the model currents follow Ekman theory at the surface and level 3 at frequencies as high as 0.90 cpd. At higher frequencies and at or below 71 m, there is little meaningful relationship between the steady Ekman response and the currents.

The phase information produced by the correlation study between the wind stress and the model currents was examined to investigate the deflection angle produced by the model's Ekman response. Only the phase angles at σ = 0.0 cycles/day corresponding to the annual signal were used, but the results are valid in the model for time scales much

greater than a day. Graphical solution techniques were employed using the spectral energy at 0.0 cpd as the magnitude of each component to determine the deflection angle between the total wind stress and the currents at the surface through level 5 (71.5 m). There is a lot of variation in the results because, though the coherence is high between the currents and their orthogonal wind stress (approximately 0.88 above 31 m), it is low in the cross-correlation between both the current components and the wind stress components themselves (about 0.18).

In the three levels examined, the phase was 0.0° between the u and v-currents; between u and the y-wind stress, and between the x-stress and the y-stress. The v-current and x-wind stress were 180° out of phase. The v-current leads both the u-current and x-wind stress. The y-wind stress leads the u-current. When the wind and current components were plotted, some interesting results were noted which confirmed the conclusions reached above. The surface current was deflected roughly 83.0° to the right of the wind stress, with the current at 31 m deflected 14.5° further for a total of 97.5° to the right of the wind. But the current at 71.5 m was approximately 24.4° to the left of

the 31 m current or 73.1° to the right of the wind. The expected Ekman spiral representation breaks down at 71.5 m. But, recall the coherence study revealed very little correlation between the wind stress and the currents at this depth. This may be a further indication that the Ekman depth in the model is above 71.5 m. It is felt this departure from Ekman theory is due to the inclusion of the geostrophic currents in this study. The geostrophic currents should be removed before any concrete conclusion is reached, but it appears from this analysis that the open ocean currents are consistent with Ekman theory at low frequency. The deflection angles near 90° are reasonable because the model assumes a well mixed upper layer (i.e. a uniform velocity, not uniform eddy viscosity) and therefore the currents equate to the mass transport at each level. They do not indicate a surface current which would be deflected 45° to the right of the wind according to Ekman theory.

C. FINE MESH INTERANNUAL COMPARISON

The major finding in the interannual comparison was that the spectral features established in the 1976-77 data remained virtually unchanged in the 1969-70 data. Just the magnitude of the spectral intensities were reduced in 1969-70.

Once again, the input wind stress was analyzed to determine if a spectral peak was present which could be reflected in the model currents, see Fig. 14. When no peak was found, a comparison was made with the 1976-77 wind data. The pattern was similar, but the spectral energy associated with the 1969-70 winds was consistently lower than its 1976-77 counterpart (except at frequencies below 0.2 cpd where the x-components were equal). This demonstrated an intensity difference in the low frequency winds from one year to another.

The reduced intensity in the spectral energy associated with the winds is reflected in the predicted model currents. The three spectral peaks associated with Ekman flow, the inertial frequency and the time differencing error at high frequency appear in both the u current, Fig. 15, and v current, Fig. 16, analyses. The inertial frequency is still shifted toward lower values compared to the frequency calculated from the coriolis parameter associated with the grid-point's latitude. The calculated inertial frequency is 1.3806 cpd while the model's inertial response is at 1.0256 cpd, as it was in the 1976-77 results. The spectral energy is reduced at all levels and is generally confined in a

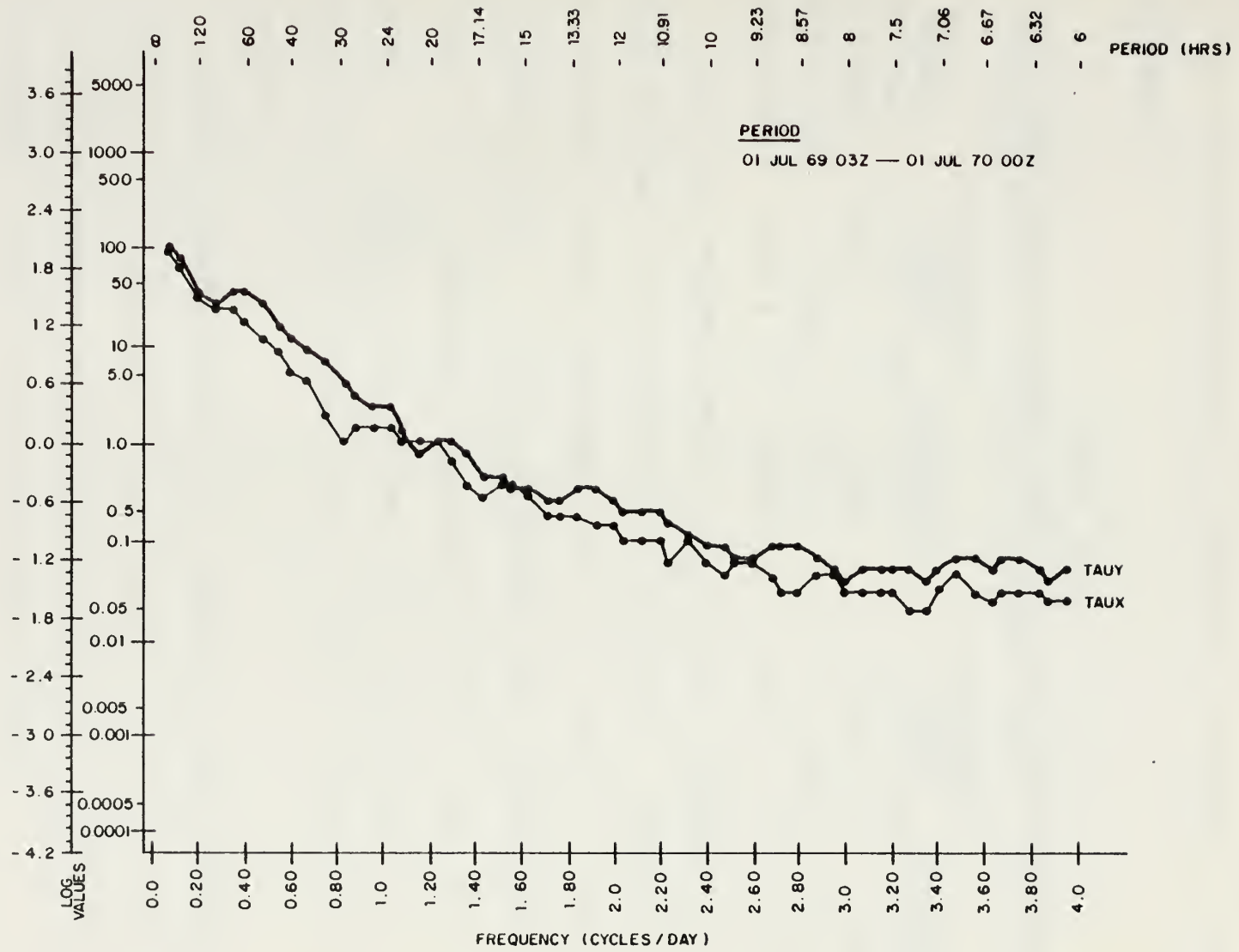

Figure 14. Energy Spectrum of Applied Wind Stress in Fine Mesh Model (JUL 69 - JUN 70).

narrower frequency band than its 1976-77 counterpart. This result is evident when the energy from half the height of the spectral peak at 1.0256 cpd and the bandwidth over which it is distributed displayed in Table II is compared to those in Table I.

TABLE II

Half Power Spectral Energy (cm^2/sec^2) and Bandwidth (cpd) for Model Inertial Motion for Fine Mesh (JUL 69 - JUN 70).

LEVEL	U-COMPONENT ENERGY	BANDWIDTH	V-COMPONENT ENERGY	BANDWIDTH
sfc (5m)	2.754×10^{2}	0.195	1.995×10^{2}	0.338
L03 (31m)	6.607×10^{1}	0.314	5.754×10^{1}	0.337
L05 (71.5m)	3.020	0.410	2.754	0.411
L10 (313m)	3.631×10^{-2}	0.246	3.631×10^{-2}	0.223

The high frequency peak is at the same frequency as the peak obtained in the 1976-77 data set study. This fact is consistent with the hypothesis that it is due to a time differencing error. The low frequency peak corresponding to Ekman flow is virtually unchanged in the two data set analyses. The RMS u and v currents are respectively: 23.5 and 20.6 cm/sec at the surface and 4.0 and 3.8 cm/sec at 71.5 m and below.

These results indicate that though the energy associated with the model depicted currents may change from year to year, its response to the forcing paramters appears to be consistent, at least in the two years analyzed.

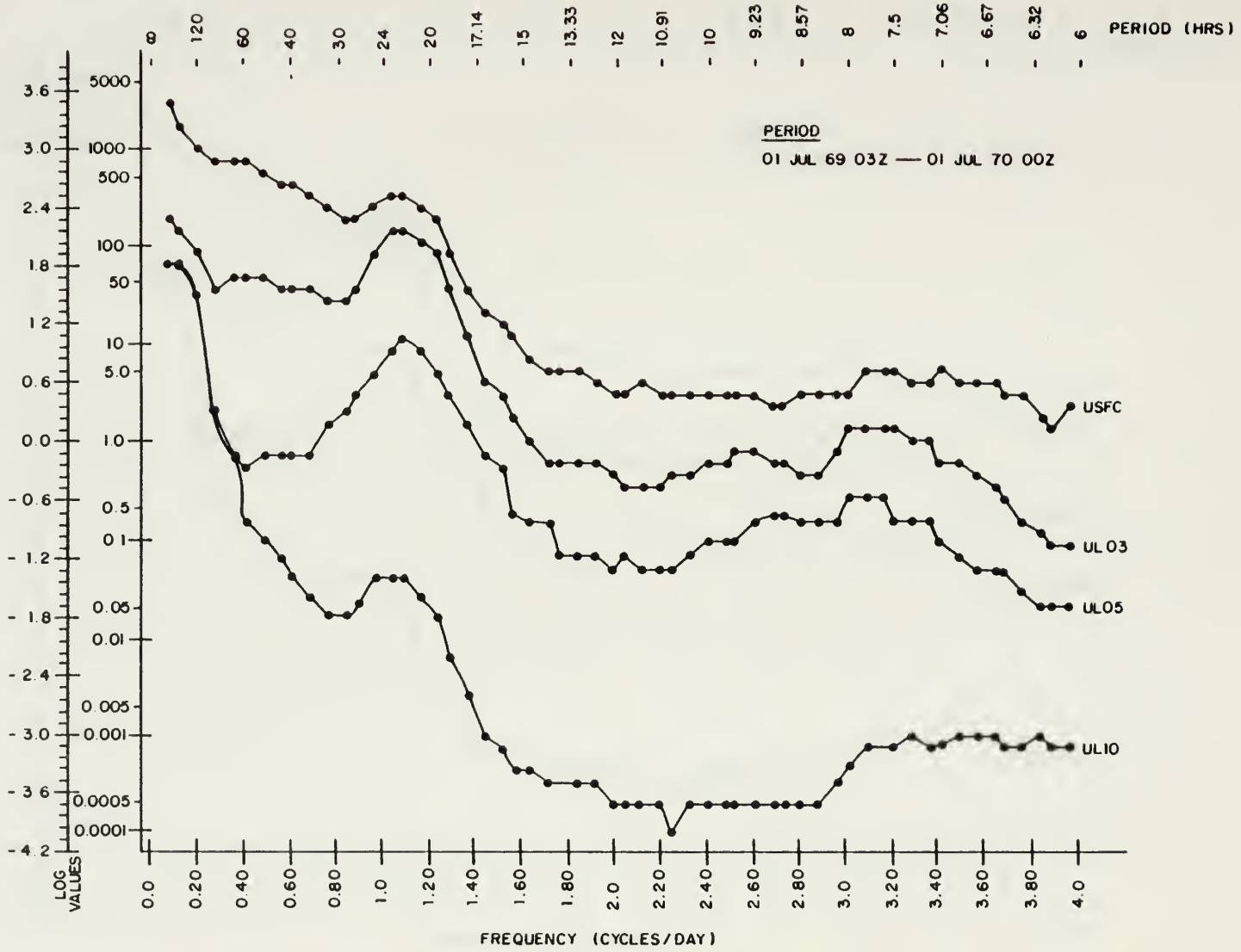

Figure 15. Energy Spectrum of U-Component Current in Fine Mesh Model (JUL 69 - JUN 70).

Figure 16. Energy Spectrum of V-Component Current in Fine Mesh Model (JUL 69 - JUN 70).

D. COARSE GRID COMPARISON

When the 1976-77 3-hourly fine mesh data were compared to its 6-hourly coarse grid counterpart, some interesting conditions were observed. The expected spectral pattern was repeated in the coarse grid analysis; but the signal associated with the spectral peaks was stornger compared to the background spectral energy than it was in the fine mesh spectral results.

The spectral peak associated with the modeled inertial response was the most dominant feature visible in both the u and v current component analyses, Figs. 17 and 18, respectively. This model characteristic is the same as the fine mesh response; but it is shifted away from the true inertial period toward even lower frequencies than the shift in the fine mesh. Recall that the calculated inertial frequency for the fine mesh gridpoint was 1.3289 cpd and the model's response was at 1.0256 cpd. In the coarse grid representation, the calculated inertial frequency is 1.3549 cpd and the model's response is at 0.7220 cpd. The results of this analysis suggest that a timestep of one (1) hour may be required to simulate the inertial motion at much more nearly the proper frequency. The energy associated with half the

height of the spectral peak at 0.722 cpd and the bandwidth over which it is distributed is displayed in Table III.

TABLE III

Half Power Spectral Energy (cm^2/sec^2) and Bandwidth (cpd) for Model Inertial Motion for Coarse Grid (JUL 76 - JUN 77).

LEVEL	U-COMPONENT ENERGY	BANDWIDTH	V-COMPONENT ENERGY	BANDWIDTH
sfc(5m)	7.079×10^{2}	0.100	5.888×10^{2}	0.123
L03(31m)	8.511×10^{1}	0.156	7.413×10^{1}	0.163
L05(71.5m)	8.710	0.168	8.710	0.123
L10(313m)	5.888×10^{-2}	0.120	6.607×10^{-2}	0.108

When the above values are compared to their fine mesh counterparts in Table I, it is noted that the energy is slightly lower but is confined in a narrower band in the coarse grid model.

The high frequency peak found at roughly 2.5 times the time step in the fine mesh run was at nearly 3 times the time step in the coarse grid run. Plus, it was amplified in the interior layers and became a dominant feature at 71.5 m. Because it was located at roughly the same point relative to the time step and its magnitude was dependent on the model resolution (including the timestep), this high frequency peak seems to be due to the time splitting characteristics of the leapfrog time differencing scheme used in the model. One approach to test this hypothesis would be to run the

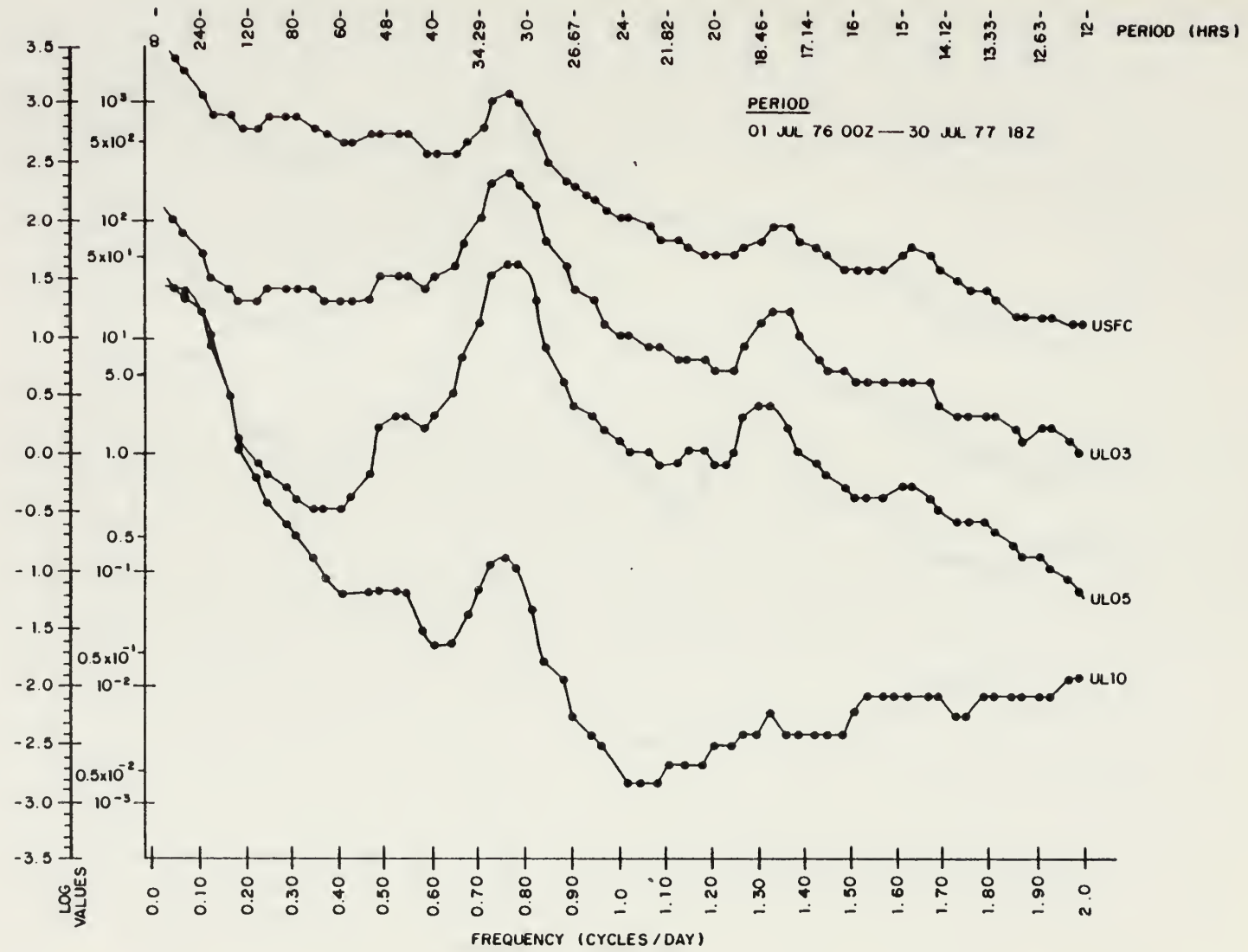

Figure 17. Energy Spectrum of U-Component Current in Coarse Grid Model (JUL 76 - JUN 77).

Figure 18. Energy Spectrum of V-Component Current in Coarse Grid Model (JUL 76 - JUN 77).

model using the Euler-backward-step every iteration rather than every eight steps, to remove the "time-splitting" in the model soultion. If this hypothesis is correct, this methcd would remove this peak from the spectral profile.

The low frequency motion is consistent with the motion displayed in the fine mesh simulation. The upper portion of the model ocean shows a baroclinic response with barotropic motion below 71.5 m. The u and v power spectrum respectively display RMS currents of the order of 23.1 and 19.4 cm/sec, respectively, at the surface and 2.5 and 1.2 cm/sec, respectively, at 71.5 m and below. These values are somewhat lower than those obtained from the fine mesh solution which is consistent with the reduced amplitudes depicted in the coarse grid inertial response.

The result of doubling the resolution is multifaceted. The frequency of the inertial motion is closer to the calculated value in the fine mesh model, but it is smeared over a broader frequency range. The effect of the high frequency "time-splitting" is reduced by increasing the resolution. The Ekman response is similar in both cases but the energy levels are slightly higher in the fine mesh simulation.

V. CONCLUSION

The Haney ocean general circulation model consistently produces three spectral peaks when analyzed over a one-year period. These peaks are located at the lowest discernible frequencies, at roughly a mid-range value and at the high frequency end. They respectively correspond to the model's Ekman response to atmospheric synoptic forcing, inertial motion and a possible numerical error due to the finite differencing method used. This overall pattern retained its structure when an interannual comparison was conducted using the fine mesh simulation. Only the magnitude of the spectral energy changed in both the analyzed input wind stress and the predicted currents. This demonstrates the variation in both atmospheric forcing and model response from year-to-year. When a comparison between the coarse grid and the fine grid was made over the same timeframe, the three-peak spectral pattern was repeated but amplified, shifted toward lower frequencies and concentrated over a narrower frequency band.

The inertial motion in the model simulation was shifted toward lower frequencies in both the fine and coarse grid representations. The frequency of the model's inertial motion was verified by a rotary spectrum analysis as determined by the minimum value of the ratio of the cyclonic to anticyclonic energy. In the 1976-77 fine grid simulation, the inertial motion was shifted approximately six hours from a true period of 18.06 h to 23.40 h in the model. In the 1969-70 data the shift was from 17.38 h to 23.40 h. This shift was even greater in the coarse grid resolution, but the inertial energy was confined to a narrower frequency range. The coarse grid response was shifted about 15.5 h from a true period of 17.71 h to 33.24 h. This shift is partially due to the stability criteria of the finite differencing scheme, which depends on $f\Delta t$. With a 3-hour time step in the fine mesh representation and an inertial period of approximately 18 hours, this accounts for roughly 3/18 or a 16% shift. A 6-hour time step in the coarse grid accounts for about 6/18 or a 33% error.

The modeled inertial motion does display some characteristics observed in the ocean. The spectral energy associated with this motion is high in the surface levels and

falls off with depth. One governing condition appears to be whether the analyzed level is above or below the seasonal thermocline. The inertial energy in the currents falls off rapidly below the surface layer. Such a decrease in inertial motion energy with depth was observed off Vancouver Island, British Columbia (Thomson and Huggett, 1981). Through the Richardson number study depicted in Figs. 3 and 4, it was demonstrated that, though the contribution may not be large, the inertial motion does add to the turbulent mixing in the model. The depth of the turbulent layer is reduced if the inertial motion was filtered out of the total model predicted currents when calculating the gradient Richardson number.

The low frequency response is consistent with Ekman flow. This was confirmed through a correlation study using lowpass filtered data. This study showed a high correlation (a coherence on the order of 0.88) between the predicted currents and the orthogonal wind stress component down to 31 m. The next level analyzed, 71.5 m, showed considerably less correlation (a coherence of 0.37) with the orthogonal winds. This matches the preliminary findings from the NORPAX drifter data which demonstrate little change in

current observations over the first 30 m of the analyzed water column. The phase information from the correlation study indicated a mass transport to the right of the wind stress as expected from Ekman Theory. The deflection angle was roughly 83° at the surface increasing to 97.5° at 31 m. But it decreased to 73.1° at 71.5 m, indicating some other physics (possibly geostrophic flow) was also involved.

To further delineate the model's current response to wind stress, the predicted currents could be divided into seasonal groups. This would allow a better study of the currents in relation to the mixed layer than can be done over an entire annual cycle. If all the levels were analyzed vice a few selected ones, the bottom of the surface response could be located and compared to the NORPAX drifter data and other current measurements in the ocean. Since the geostrophic current components can be calculated exactly by the model, they could be subtracted from the total currents leaving the ageostrophic current. This ageostrophic field could then be analyzed to investigate the model's characteristics in the realm of Ekman dynamics. The curl of the wind stress could also be calculated to determine areas of Ekman suction and pumping. Plus, complex transfer functions could give an indication of their frequency dependence.

The high frequency peak found in the spectral results was unexpected. It is located at a period roughly 2.5 times the time step in the fine mesh model and displays vigorous cyclonic motion. In the coarse grid resolution, it is shifted to approximately three times the time step. Its amplitude is magnified in the coarser resolution configuration. A possible explanation is that it is related to the "time splitting" problems inherent with the leapfrog time differencing scheme. To test this hypothesis, an Euler-backward procedure could be inserted every time step to damp out this "time splitting" in the numerical solution. This would remove this peak from the spectrum. It should be noted that the energy level associated with this time splitting is very small in comparison with the currents simulated in the model.

Further investigation is required to fully understand this model's circulation characteristics. Once analysis of the NORPAX drifter data is complete, a verification of the model's performance should be conducted. The results of these studies will validate the model and make it a viable tool in understanding the structure and time-varying general circulation of the North Pacific.

APPENDIX A

The following tables show the results of the rotary spectrum analysis performed on the 1976-77 fine mesh data set. The model and theoretical values displayed in these results are from a ratio of the cyclonic to anticyclonic components in the motion analyzed. The larger the value listed, the stronger the cyclonic motion at that particular frequency. Recall from theory that a value of zero equates to the inertial frequency while a value of one corresponds to rectilinear motion. the variables presented in the following tables correspond to:

FREQ = frequency (cycles/day)

GUU = u-current autospectrum

GVV = v-current autospectrum

QUV = quadrature or imaginary cross spectrum of u and v

MODEL = model rotary spectrum (equation 2)

THEORY = theoretical rotary spectrum (equation 3)

TABLE IV

Rotary Spectrum Results for Surface (5 m), Fine Mesh Data (JUN 1976 - JUL 1977).

FREQ	GUU	GVV	QUV	MODEL	THEORY
0.068	0.265E+04	0.176E+04	-0.233E+03	0.809E+00	0.815E+00
0.137	0.148E+04	0.104E+04	-0.264E+03	0.655E+00	0.662E+00
0.205	0.132E+04	0.605E+03	-0.314E+03	0.508E+00	0.537E+00
0.274	0.126E+04	0.458E+04	-0.318E+03	0.804E+00	0.434E+00
0.342	0.106E+04	0.474E+03	-0.373E+03	0.347E+00	0.349E+00
0.410	0.914E+03	0.530E+03	-0.467E+03	0.214E+00	0.279E+00
0.478	0.805E+03	0.521E+03	-0.493E+03	0.147E+00	0.221E+00
0.547	0.603E+03	0.354E+03	-0.341E+03	0.168E+00	0.174E+00
0.615	0.433E+03	0.214E+03	-0.182E+03	0.279E+00	0.135E+00
0.684	0.403E+03	0.295E+03	-0.250E+03	0.165E+00	0.103E+00
0.752	0.443E+03	0.339E+03	-0.350E+03	0.551E-01	0.769E-01
0.821	0.566E+03	0.458E+03	-0.465E+03	0.479E-01	0.559E-01
0.889	0.758E+03	0.621E+03	-0.654E+03	0.268E-01	0.394E-01
0.958	0.980E+03	0.848E+03	-0.871E+03	0.239E-01	0.264E-01
1.026	0.962E+03	0.859E+03	-0.872E+03	0.215E-01	0.166E-01
1.094	0.642E+03	0.581E+03	-0.584E+03	0.228E-01	0.936E-02
1.162	0.328E+03	0.303E+03	-0.295E+03	0.342E-01	0.447E-02
1.230	0.155E+03	0.156E+03	-0.140E+03	0.505E-01	0.148E-02
1.299	0.951E+02	0.963E+02	-0.839E+02	0.658E-01	0.128E-03
1.367	0.669E+02	0.661E+02	-0.549E+02	0.948E-01	0.202E-03
1.436	0.406E+02	0.409E+02	-0.311E+02	0.135E+00	0.150E-02
1.504	0.242E+02	0.307E+02	-0.188E+02	0.186E+00	0.382E-02
1.573	0.172E+02	0.294E+02	-0.142E+02	0.242E+00	0.707E-02
1.641	0.125E+02	0.218E+02	-0.825E+01	0.349E+00	0.110E-01
1.710	0.101E+02	0.175E+02	-0.495E+01	0.471E+00	0.157E-01
1.778	0.890E+01	0.160E+02	-0.371E+01	0.542E+00	0.209E-01
1.846	0.796E+01	0.126E+02	-0.217E+01	0.652E+00	0.266E-01
1.914	0.756E+01	0.103E+02	-0.539E+00	0.886E+00	0.326E-01
1.983	0.714E+01	0.935E+01	-0.545E+00	0.876E+00	0.390E-01
2.051	0.707E+01	0.854E+01	-0.134E+01	0.708E+00	0.457E-01
2.120	0.629E+01	0.771E+01	-0.108E+01	0.733E+00	0.526E-01
2.188	0.517E+01	0.843E+01	-0.184E+00	0.947E+00	0.597E-01
2.257	0.506E+01	0.827E+01	0.127E+01	0.147E+01	0.670E-01
2.325	0.555E+01	0.663E+01	0.201E+01	0.198E+01	0.743E-01
2.393	0.536E+01	0.607E+01	0.201E+01	0.208E+01	0.817E-01
2.462	0.451E+01	0.593E+01	0.213E+01	0.238E+01	0.893E-01
2.530	0.400E+01	0.545E+01	0.259E+01	0.343E+01	0.968E-01
2.598	0.481E+01	0.611E+01	0.350E+01	0.458E+01	0.104E+00
2.666	0.535E+01	0.559E+01	0.346E+01	0.445E+01	0.112E+00
2.735	0.440E+01	0.469E+01	0.282E+01	0.426E+01	0.120E+00
2.803	0.374E+01	0.464E+01	0.267E+01	0.450E+01	0.127E+00
2.872	0.477E+01	0.513E+01	0.347E+01	0.570E+01	0.135E+00
2.940	0.818E+01	0.892E+01	0.679E+01	0.871E+01	0.142E+00
3.009	0.110E+02	0.134E+02	0.995E+01	0.983E+01	0.150E+00
3.077	0.113E+02	0.139E+02	0.107E+02	0.123E+02	0.157E+00
3.146	0.991E+01	0.110E+02	0.902E+01	0.136E+02	0.165E+00
3.214	0.875E+01	0.890E+01	0.722E+01	0.999E+01	0.172E+00
3.282	0.807E+01	0.732E+01	0.603E+01	0.825E+01	0.179E+00
3.350	0.689E+01	0.490E+01	0.399E+01	0.520E+01	0.187E+00
3.418	0.630E+01	0.395E+01	0.309E+01	0.402E+01	0.194E+00
3.487	0.624E+01	0.521E+01	0.400E+01	0.562E+01	0.201E+00
3.555	0.538E+01	0.534E+01	0.397E+01	0.672E+01	0.208E+00
3.624	0.416E+01	0.385E+01	0.278E+01	0.553E+01	0.215E+00
3.692	0.354E+01	0.252E+01	0.181E+01	0.397E+01	0.222E+00
3.761	0.265E+01	0.172E+01	0.105E+01	0.285E+01	0.228E+00
3.829	0.208E+01	0.190E+01	0.886E+00	0.260E+01	0.235E+00
3.898	0.367E+01	0.281E+01	0.999E+00	0.189E+01	0.242E+00
3.966	0.925E+01	0.559E+01	0.534E+00	0.116E+01	0.248E+00

TABLE V

Rotary Spectrum Results for Level 3 (31 m), Fine Mesh Data (JUN 1976 - JUL 1977).

FREQ	GUU	GVV	QUV	MODEL	THEORY
0.068	0.151E+03	0.117E+03	-0.493E+01	0.929E+00	0.815E+00
0.137	0.738E+02	0.553E+02	-0.964E+01	0.740E+00	0.662E+00
0.205	0.489E+02	0.296E+02	-0.150E+02	0.448E+00	0.537E+00
0.274	0.516E+02	0.275E+02	-0.194E+02	0.342E+00	0.434E+00
0.342	0.515E+02	0.294E+02	-0.253E+02	0.231E+00	0.349E+00
0.410	0.480E+02	0.272E+02	-0.283E+02	0.141E+00	0.279E+00
0.478	0.445E+02	0.284E+02	-0.305E+02	0.887E-01	0.221E+00
0.547	0.377E+02	0.248E+02	-0.269E+02	0.753E-01	0.174E+00
0.615	0.338E+02	0.229E+02	-0.240E+02	0.844E-01	0.135E+00
0.684	0.449E+02	0.387E+02	-0.386E+02	0.401E-01	0.103E+00
0.752	0.615E+02	0.557E+02	-0.564E+02	0.186E-01	0.769E-01
0.821	0.988E+02	0.884E+02	-0.919E+02	0.897E-02	0.559E-01
0.889	0.171E+03	0.157E+03	-0.163E+03	0.398E-02	0.394E-01
0.958	0.243E+03	0.231E+03	-0.236E+03	0.285E-02	0.264E-01
1.026	0.237E+03	0.232E+03	-0.233E+03	0.278E-02	0.166E-01
1.094	0.154E+03	0.150E+03	-0.151E+03	0.346E-02	0.936E-02
1.162	0.744E+02	0.709E+02	-0.718E+02	0.616E-02	0.447E-02
1.230	0.293E+02	0.283E+02	-0.281E+02	0.125E-01	0.148E-02
1.299	0.125E+02	0.118E+02	-0.116E+02	0.239E-01	0.128E-03
1.367	0.887E+01	0.827E+01	-0.801E+01	0.338E-01	0.202E-03
1.436	0.539E+01	0.513E+01	-0.474E+01	0.519E-01	0.150E-02
1.504	0.286E+01	0.283E+01	-0.240E+01	0.843E-01	0.382E-02
1.573	0.182E+01	0.213E+01	-0.153E+01	0.128E+00	0.707E-02
1.641	0.120E+01	0.161E+01	-0.954E+00	0.192E+00	0.110E-01
1.710	0.105E+01	0.122E+01	-0.691E+00	0.243E+00	0.157E-01
1.778	0.104E+01	0.999E+00	-0.560E+00	0.290E+00	0.209E-01
1.846	0.954E+00	0.814E+00	-0.434E+00	0.342E+00	0.266E-01
1.914	0.761E+00	0.797E+00	-0.300E+00	0.444E+00	0.326E-01
1.983	0.682E+00	0.764E+00	-0.233E+00	0.513E+00	0.390E-01
2.051	0.712E+00	0.589E+00	-0.169E+00	0.588E+00	0.457E-01
2.120	0.742E+00	0.494E+00	-0.870E-01	0.753E+00	0.526E-01
2.188	0.742E+00	0.531E+00	0.223E-01	0.107E+01	0.597E-01
2.257	0.621E+00	0.586E+00	0.141E+00	0.161E+01	0.670E-01
2.325	0.524E+00	0.563E+00	0.176E+00	0.196E+01	0.743E-01
2.393	0.512E+00	0.501E+00	0.222E+00	0.257E+01	0.817E-01
2.462	0.473E+00	0.438E+00	0.250E+00	0.344E+01	0.893E-01
2.530	0.426E+00	0.423E+00	0.220E+00	0.316E+01	0.968E-01
2.598	0.422E+00	0.480E+00	0.218E+00	0.287E+01	0.104E+00
2.666	0.504E+00	0.597E+00	0.249E+00	0.265E+01	0.112E+00
2.735	0.582E+00	0.667E+00	0.323E+00	0.314E+01	0.120E+00
2.803	0.551E+00	0.659E+00	0.380E+00	0.437E+01	0.127E+00
2.872	0.707E+00	0.791E+00	0.540E+00	0.618E+01	0.135E+00
2.940	0.122E+01	0.132E+01	0.994E+00	0.818E+01	0.142E+00
3.009	0.157E+01	0.194E+01	0.145E+01	0.103E+02	0.150E+00
3.077	0.137E+01	0.195E+01	0.139E+01	0.114E+02	0.157E+00
3.146	0.102E+01	0.137E+01	0.973E+00	0.974E+01	0.165E+00
3.214	0.902E+00	0.964E+00	0.740E+00	0.869E+01	0.172E+00
3.282	0.791E+00	0.776E+00	0.624E+00	0.880E+01	0.179E+00
3.350	0.700E+00	0.580E+00	0.472E+00	0.662E+01	0.187E+00
3.418	0.628E+00	0.437E+00	0.360E+00	0.517E+01	0.194E+00
3.487	0.508E+00	0.419E+00	0.313E+00	0.516E+01	0.201E+00
3.555	0.429E+00	0.415E+00	0.267E+00	0.446E+01	0.208E+00
3.624	0.363E+00	0.376E+00	0.214E+00	0.375E+01	0.215E+00
3.692	0.270E+00	0.311E+00	0.154E+00	0.324E+01	0.222E+00
3.761	0.204E+00	0.212E+00	0.775E-01	0.219E+01	0.228E+00
3.829	0.192E+00	0.221E+00	0.620E-01	0.186E+01	0.235E+00
3.898	0.214E+00	0.254E+00	0.540E-01	0.160E+01	0.242E+00
3.966	0.357E+00	0.222E+00	0.188E-01	0.114E+01	0.248E+00

TABLE VI

Rotary Spectrum Results for Level 5 (71.5 m), Fine Mesh Data (JUN 1976 - JUL 1977).

FREQ	GUU	GVV	QUV	MODEL	THEORY
0.068	0.568E+02	0.380E+02	0.364E+01	0.117E+01	0.815E+00
0.137	0.184E+02	0.254E+02	0.226E+01	0.123E+01	0.662E+00
0.205	0.220E+01	0.708E+01	-0.257E+00	0.895E+00	0.537E+00
0.274	0.102E+01	0.241E+01	-0.305E+00	0.698E+00	0.434E+00
0.342	0.108E+01	0.165E+01	-0.662E+00	0.346E+00	0.349E+00
0.410	0.174E+01	0.190E+01	-0.136E+01	0.145E+00	0.279E+00
0.478	0.234E+01	0.208E+01	-0.182E+01	0.958E-01	0.221E+00
0.547	0.206E+01	0.175E+01	-0.160E+01	0.867E-01	0.174E+00
0.615	0.166E+01	0.161E+01	-0.130E+01	0.114E+00	0.135E+00
0.684	0.309E+01	0.360E+01	-0.312E+01	0.343E-01	0.103E+00
0.752	0.596E+01	0.685E+01	-0.627E+01	0.108E-01	0.769E-01
0.821	0.135E+02	0.142E+02	-0.137E+02	0.417E-02	0.559E-01
0.889	0.325E+02	0.321E+02	-0.322E+02	0.132E-02	0.394E-01
0.958	0.547E+02	0.521E+02	-0.533E+02	0.890E-03	0.264E-01
1.026	0.558E+02	0.523E+02	-0.539E+02	0.926E-03	0.166E-01
1.094	0.337E+02	0.332E+02	-0.324E+02	0.153E-01	0.936E-02
1.162	0.125E+02	0.116E+02	-0.120E+02	0.396E-02	0.447E-02
1.230	0.380E+01	0.391E+01	-0.378E+01	0.976E-02	0.148E-02
1.299	0.206E+01	0.233E+01	-0.213E+01	0.153E-01	0.128E-03
1.367	0.115E+01	0.144E+01	-0.123E+01	0.254E-01	0.202E-03
1.436	0.598E+00	0.810E+00	-0.637E+00	0.504E-01	0.150E-02
1.504	0.372E+00	0.570E+00	-0.393E+00	0.896E-01	0.382E-02
1.573	0.330E+00	0.498E+00	-0.327E+00	0.117E+00	0.707E-02
1.641	0.259E+00	0.324E+00	-0.207E+00	0.169E+00	0.110E-01
1.710	0.208E+00	0.197E+00	-0.123E+00	0.243E+00	0.157E-01
1.778	0.178E+00	0.147E+00	-0.893E-01	0.290E+00	0.209E-01
1.846	0.155E+00	0.865E-01	-0.582E-01	0.350E+00	0.266E-01
1.914	0.147E+00	0.822E-01	-0.455E-01	0.432E+00	0.326E-01
1.983	0.116E+00	0.871E-01	-0.353E-01	0.485E+00	0.390E-01
2.051	0.114E+00	0.722E-01	-0.269E-01	0.552E+00	0.457E-01
2.120	0.126E+00	0.744E-01	-0.150E-01	0.739E+00	0.526E-01
2.188	0.114E+00	0.801E-01	0.525E-02	0.111E+01	0.597E-01
2.257	0.105E+00	0.727E-01	0.176E-01	0.149E+01	0.670E-01
2.325	0.103E+00	0.779E-01	0.490E-02	0.111E+01	0.743E-01
2.393	0.960E-01	0.925E-01	0.836E-02	0.119E+01	0.817E-01
2.462	0.736E-01	0.115E+00	0.301E-01	0.194E+01	0.893E-01
2.530	0.620E-01	0.124E+00	0.388E-01	0.243E+01	0.968E-01
2.598	0.765E-01	0.939E-01	0.403E-01	0.280E+01	0.104E+00
2.666	0.873E-01	0.629E-01	0.308E-01	0.239E+01	0.112E+00
2.735	0.913E-01	0.688E-01	0.254E-01	0.193E+01	0.120E+00
2.803	0.118E+00	0.101E+00	0.525E-01	0.284E+01	0.127E+00
2.872	0.167E+00	0.164E+00	0.114E+00	0.542E+01	0.135E+00
2.940	0.250E+00	0.246E+00	0.206E+00	0.109E+02	0.142E+00
3.009	0.355E+00	0.324E+00	0.299E+00	0.159E+02	0.150E+00
3.077	0.347E+00	0.322E+00	0.290E+00	0.141E+02	0.157E+00
3.146	0.220E+00	0.205E+00	0.170E+00	0.909E+01	0.165E+00
3.214	0.151E+00	0.154E+00	0.117E+00	0.764E+01	0.172E+00
3.282	0.137E+00	0.151E+00	0.112E+00	0.811E+01	0.179E+00
3.350	0.105E+00	0.112E+00	0.573E-01	0.324E+01	0.187E+00
3.418	0.107E+00	0.908E-01	0.388E-01	0.229E+01	0.194E+00
3.487	0.120E+00	0.731E-01	0.507E-01	0.321E+01	0.201E+00
3.555	0.890E-01	0.676E-01	0.407E-01	0.316E+01	0.208E+00
3.624	0.573E-01	0.729E-01	0.276E-01	0.247E+01	0.215E+00
3.692	0.476E-01	0.516E-01	0.123E-01	0.166E+01	0.222E+00
3.761	0.481E-01	0.316E-01	0.412E-02	0.123E+01	0.228E+00
3.829	0.562E-01	0.417E-01	-0.149E-02	0.941E+00	0.235E+00
3.898	0.566E-01	0.671E-01	-0.835E-02	0.762E+00	0.242E+00
3.966	0.495E-01	0.709E-01	-0.459E-02	0.858E+00	0.248E+00

TABLE VII

Rotary Spectrum Results for Level 10 (313 m), Fine Mesh Data (JUN 1976 - JUL 1977).

FREQ	GUU	GVV	QUV	MODEL	THEORY
0.068	0.587E+02	0.395E+02	0.232E+02	0.279E+01	0.815E+00
0.137	0.181E+02	0.248E+02	0.108E+02	0.303E+01	0.662E+00
0.205	0.173E+02	0.554E+02	-0.756E+00	0.959E+00	0.537E+00
0.274	0.466E+00	0.989E+00	-0.426E+00	0.261E+00	0.434E+00
0.342	0.215E+00	0.365E+00	-0.185E+00	0.222E+00	0.349E+00
0.410	0.146E+00	0.181E+00	-0.123E+00	0.140E+00	0.279E+00
0.478	0.109E+00	0.130E+00	-0.961E-01	0.108E+00	0.221E+00
0.547	0.636E-01	0.796E-01	-0.572E-01	0.112E+00	0.174E+00
0.615	0.327E-01	0.450E-01	-0.287E-01	0.151E+00	0.135E+00
0.684	0.393E-01	0.411E-01	-0.336E-01	0.890E-01	0.103E+00
0.752	0.473E-01	0.451E-01	-0.421E-01	0.456E-01	0.769E-01
0.821	0.587E-01	0.586E-01	-0.554E-01	0.284E-01	0.559E-01
0.889	0.849E-01	0.837E-01	-0.811E-01	0.188E-01	0.394E-01
0.958	0.116E+00	0.109E+00	-0.109E+00	0.144E-01	0.264E-01
1.026	0.110E+00	0.104E+00	-0.104E+00	0.135E-01	0.166E-01
1.094	0.609E-01	0.601E-01	-0.580E-01	0.209E-01	0.936E-02
1.162	0.219E-01	0.233E-01	-0.204E-01	0.510E-01	0.447E-02
1.230	0.831E-02	0.897E-02	-0.673E-02	0.125E+00	0.148E-02
1.299	0.385E-02	0.464E-02	-0.253E-02	0.253E+00	0.128E-03
1.367	0.237E-02	0.331E-02	-0.139E-02	0.341E+00	0.202E-03
1.436	0.146E-02	0.217E-02	-0.651E-03	0.471E+00	0.150E-02
1.504	0.952E-03	0.167E-02	-0.262E-03	0.668E+00	0.382E-02
1.573	0.813E-03	0.153E-02	-0.265E-03	0.631E+00	0.707E-02
1.641	0.627E-03	0.129E-02	-0.316E-03	0.505E+00	0.110E-01
1.710	0.499E-03	0.114E-02	-0.357E-03	0.392E+00	0.157E-01
1.778	0.442E-03	0.103E-02	-0.370E-03	0.330E+00	0.209E-01
1.846	0.389E-03	0.820E-03	-0.304E-03	0.331E+00	0.266E-01
1.914	0.489E-03	0.618E-03	-0.303E-03	0.292E+00	0.326E-01
1.983	0.585E-03	0.572E-03	-0.369E-03	0.221E+00	0.390E-01
2.051	0.553E-03	0.483E-03	-0.346E-03	0.199E+00	0.457E-01
2.120	0.537E-03	0.335E-03	-0.277E-03	0.224E+00	0.526E-01
2.188	0.589E-03	0.254E-03	-0.186E-03	0.389E+00	0.597E-01
2.257	0.601E-03	0.228E-03	-0.541E-04	0.769E+00	0.670E-01
2.325	0.561E-03	0.214E-03	0.280E-04	0.116E+01	0.743E-01
2.393	0.562E-03	0.191E-03	0.895E-04	0.162E+01	0.817E-01
2.462	0.557E-03	0.176E-03	0.130E-03	0.210E+01	0.893E-01
2.530	0.509E-03	0.184E-03	0.153E-03	0.259E+01	0.968E-01
2.598	0.480E-03	0.248E-03	0.213E-03	0.381E+01	0.104E+00
2.666	0.443E-03	0.315E-03	0.259E-03	0.529E+01	0.112E+00
2.735	0.464E-03	0.356E-03	0.292E-03	0.596E+01	0.120E+00
2.803	0.486E-03	0.373E-03	0.296E-03	0.543E+01	0.127E+00
2.872	0.397E-03	0.445E-03	0.279E-03	0.492E+01	0.135E+00
2.940	0.504E-03	0.781E-03	0.453E-03	0.577E+01	0.142E+00
3.009	0.767E-03	0.109E-02	0.671E-03	0.626E+01	0.150E+00
3.077	0.796E-03	0.111E-02	0.649E-03	0.525E+01	0.157E+00
3.146	0.731E-03	0.113E-02	0.549E-03	0.388E+01	0.165E+00
3.214	0.844E-03	0.113E-02	0.567E-03	0.370E+01	0.172E+00
3.282	0.834E-03	0.157E-02	0.549E-03	0.258E+01	0.179E+00
3.350	0.713E-03	0.156E-02	0.425E-03	0.219E+01	0.187E+00
3.418	0.744E-03	0.160E-02	0.360E-03	0.188E+01	0.194E+00
3.487	0.831E-03	0.182E-02	0.479E-03	0.213E+01	0.201E+00
3.555	0.976E-03	0.177E-02	0.496E-03	0.213E+01	0.208E+00
3.624	0.106E-02	0.142E-02	0.296E-03	0.163E+01	0.215E+00
3.692	0.910E-03	0.115E-02	0.715E-04	0.115E+01	0.222E+00
3.761	0.827E-03	0.103E-02	-0.640E-04	0.871E+00	0.228E+00
3.829	0.787E-03	0.120E-02	-0.117E-03	0.790E+00	0.235E+00
3.898	0.736E-03	0.148E-02	-0.652E-04	0.889E+00	0.242E+00
3.966	0.631E-03	0.198E-02	0.795E-05	0.101E+01	0.248E+00

LIST OF REFERENCES

Adamec, D., Elsberry, R. L., Garwood, R. W. Jr., and Haney, R. L., 1981: "An Embedded Mixed-Layer Ocean Circulation Model", Dyn. Atmos. Oceans, 6, 69-96.

Bendat, J. S. and Piersol, A. G., 1971: Random Data: Analysis and Measurement Procedures. New York, N. Y.: Wiley-Interscience of Wiley and Sons Inc., 407 pp.

DeSzoeke, R. A., 1980: "On the Effects of Horizontal Variability of Wind Stress on the Dynamics of the Ocean Mixed Layer", J. Phys. Oceanogr., 10, 1439-1454.

Engelman, E., Frane, J. W., and Jennrich, R. I., 1981: BMDP Biomedical Computer Programs, P-series, 1981., Berkeley, Ca: University of California Press., pp. 604-637, 686-689.

Haney, R. L., Shiver, W. S., and Hunt, K. H., 1978: "A Dymanical-Numerical Study of the Formation and Evolution of Large-Scale Ocean Anomalies", J. Phys. Oceanogr., 8, 952-969.

_____, 1980: "A Numerical Case Study of the Development of Large-Scale Thermal Anomalies in the Central North Pacific Ocean", J. Phys. Oceanogr., 10, 541-556.

McNally, G. J., 1981: "Satellite-Tracked Drift Buoy Observations of the Near-Surface Flow in the Eastern Mid-Latitude North Pacific", J. Geophys. Res., 86, 8022-8030.

Mooers, C. N. K., 1973: "A Technique for the Cross Spectrum Analysis of Pairs of Complex-Valued Time Series, with Emphasis on Properties of Polarized Components and Rotational Invariants", Deep-Sea Res., 20, 1129-1141.

Neumann, G. and Pierson, W. J. Jr., 1966: Principles of Physical Oceanography. Englewood Cliffs, N.J.: Prentice-Hall Inc., 545 pp.

Sverdrup, H. U., Johnson, M. W., and Fleming, R. H., 1942: The Oceans Their Physics, Chemistry and General Biology. Englewood Cliffs, N. J.: Prentice-Hall Inc., 1087 pp.

Thompson, R. O. R. Y., 1980: "Efficency of Conversion of Kinetic Energy to Potential Energy by a Breaking Internal Gravity Wave", J. Geophys. Res., 85, 6631-6635.

Thomson, R. E., and Huggett, W. S., 1981: "Wind-Driven Inertial Oscillations of Large Spatial Coherence", Atmos.-Ocean, 19, 281-306.

Weatherly, G. L., 1972: "A Study of the Bottom Boundary Layer of the Florida Current", J. Phys. Oceanogr., 2, 54-72.

INITIAL DISTRIBUTION LIST

		No. Copies
1.	Defense Technical Information Center Cameron Station Alexandria, VA 22314	2
2.	Library, Code 0142 Naval Postgraduate School Monterey, CA 93940	2
3.	Professor C.N.K Mooers, Code 68Mr Naval Postgraduate School Monterey, CA 93940	1
4.	Professor R.J. Renard, Code 63Rd Naval Postgraduate School Monterey, CA 93940	1
5.	Professor R.L. Haney, Code 63Hy Naval Postgraduate School Monterey, CA 93940	1
6.	Reference Library Department of Meteorology, Code 63 Naval Postgradute School Monterey, CA 93940	1
7.	Director Naval Oceanography Division Naval Observatory 34th and Massachusetts Ave. NW Washington, D.C. 20390	1
8.	Commander Naval Oceanography Command NSTL Station Bay St. Louis, MS 39522	1
9.	Commanding Officer Naval Oceanographic Office NSTL Station Bay St. Louis, MS 39522	1
10.	Commanding Officer Fleet Numerical Oceanography Center Monterey, CA 93940	1
11.	Commanding Officer Naval Ocean Research and Development Activity NSTL Station Bay St. Louis, MS 39522	1

12. Commanding Officer 1
Naval Environmental Prediction Research Facility
Monterey, CA 93940

13. Chairman, Oceanography Department 1
U.S. Naval Academy
Anapolis, MD 21402

14. Chief of Naval Research 1
800 N. Quincy Street
Arlington, VA 22217

15. Office of Naval Research (Code 480) 1
Naval Oceanography Research and Development
Activity
NSTL Station
Bay St. Louis, MS 39522

16. Scientific Liaison Office 1
Office of Naval Research
Scripps Institute of Oceanography
La Jolla, CA 92037

17. Dr. G. J. McNally 1
NORPAX A-030
Scripps Institute of Oceanography
La Jolla, CA 92037

18. Library 1
Scripps Institute of Oceanography
P.O. Box 2367
La Jolla, CA 92037

19. Library 1
Department of Oceanography
University of Washington
Seattle, WA 98105

20. Library 1
CICESE
P.O. Box 4803
San Ysidro, CA 92073

21. Library 1
School of Oceanography
Oregon State University
Corvallis, OR 97331

22. Commander 1
Oceanographic Systems Pacific
Box 1390
Pearl Harbor, HI 96860

23. Lt. Nicholas D. Gural 2
Navoceancomfac, Yokosuka
Box 68
FPO Seattle, Wa 98762

200078

Thesis
G8766 Gural
c.1

Spectrum analysis of inertial and sub-inertial motions based on analyzed winds and wind-driven currents from a primitive equation general ocean circulation model.